The Astronomical Journal, 164:171 (17pp), 2022 November https://doi.org/10.3847/1538-3881/ac8cf4

A Comprehensive Study of Five Intermediate-age Pismis (2, 3, 7, 12, 15) Clusters Using Photometric and Astrometric Data from Gaia EDR3

D. Bisht[1], Qingfeng Zhu[1], W. H. Elsanhoury[2,3], R. K. S. Yadav[4], Geeta Rangwal[5], Devesh P. Sariya[6], Alok Durgapal[7], and Ing-Guey Jiang[6]

[1] Key Laboratory for Researches in Galaxies and Cosmology, University of Science and Technology of China, Chinese Academy of Sciences, Hefei, Anhui, 230026, People's Republic of China; dbisht@ustc.edu.cn
[2] Astronomy Department, National Research Institute of Astronomy and Geophysics (NRIAG), 11421, Helwan, Cairo, Egypt
[3] Physics Department, Faculty of Science and Arts, Northern Border University, Turaif Branch, Saudi Arabia
[4] Aryabhatta Research Institute of Observational Sciences, Manora Peak, Nainital, 263 002, India
[5] Indian Institute of Astrophysics, Koramangala II Block, Bangalore, 560034, India
[6] Department of Physics and Institute of Astronomy, National Tsing-Hua University, Hsin-Chu, Taiwan
[7] Center of Advanced Study, Department of Physics, D. S. B. Campus, Kumaun University, Nainital, 263002, India
Received 2022 May 16; revised 2022 August 24; accepted 2022 August 24; published 2022 October 4

Abstract

Open clusters are groups of stars that form simultaneously; hence, these are excellent probes to test theories of star formation, stellar evolution, and dynamics in the Milky Way disk. We carry out a detailed photometric and kinematic study of five poorly studied intermediate-age open clusters, Pismis 2 (Pi 2), Pismis 3 (Pi 3), Pismis 7 (Pi 7), Pismis 12 (Pi 12), and Pismis 15 (Pi 15), using the Gaia EDR3 database. By estimating the membership probabilities of stars, we recognized 635, 1488, 535, 368, and 494 most probable members for these clusters by using proper-motion and parallax data taken from Gaia EDR3. The radial density profiles of cluster members provide cluster radii of 4.′5–6.′5 for these clusters. Their ages range from 0.9 to 2.5 Gyr, and distances range, using parallax, from 2.15 to 5.10 kpc. The overall mass function slopes for main-sequence stars are found as 0.27 ± 0.16 (for 1.0–1.6 $M_{\odot}$ stars), 0.86 ± 0.27 (for 1.0–2.1 $M_{\odot}$ stars), 1.08 ± 0.32 (for 1.0–2.2 $M_{\odot}$ stars), 0.89 ± 0.38 (for 1.0–2.2 $M_{\odot}$ stars), and 1.07 ± 0.28 (for 1.0–2.1 $M_{\odot}$ stars) for clusters Pi 2, Pi 3, Pi 7, Pi 12, and Pi 15. Our obtained values of slopes are flatter in comparison with Salpeter's value ($x = 1.35$) within uncertainty. The present study demonstrates that all these Pismis clusters are dynamically relaxed. We found that these objects follow a circular path around the Galactic center. We compute these clusters' apex coordinates (A, D) and other kinematic parameters.

Unified Astronomy Thesaurus concepts: Open star clusters (1160); Initial mass function (796); Stellar dynamics (1596); Stellar kinematics (1608); Orbits (1184); Proper motions (1295)

1. Introduction

Open clusters (OCs) cover a broad range of ages, from a few million to billions of years. OCs are fundamental objects to understanding the star formation process and stellar evolution (Lada & Lada 2003; Portegies Zwart et al. 2010). OCs, particularly the intermediate/old ones, are good laboratories for verifying stellar evolution theories (Kim et al. 2017). They are also valuable tracers to examine the structure and dynamical evolution of the Galaxy (e.g., Friel 1995; Xu et al. 2018; Cantat-Gaudin et al. 2020; He et al. 2021; Hou 2021). The fundamental parameters of OCs have been listed in several catalogs (Dias et al. 2002; Röser et al. 2010; Kharchenko et al. 2013; Dias et al. 2014; Sampedro et al. 2017; Cantat-Gaudin et al. 2018; Soubiran et al. 2018; Cantat-Gaudin et al. 2020).

A precise membership and physical parameter determination are beneficial in studying mass distribution during the formation of stars, known as the initial mass function (IMF). Whether the IMF is universal in time and space or depends on different star-forming conditions is still debated (Larson 1998; Bastian et al. 2010; Dib & Basu 2018; Jeřábková et al. 2018).

The apex coordinates are essential parameters in the kinematic and physical examination of stars and clusters (Wayman et al. 1965; Hanson 1975; Eggen 1984; Gunn et al. 1988). For this purpose, numerous techniques are available in the literature, such as (i) the classical convergent point method, (ii) the AD chart method, and (iii) the convergent point search method (CPSM; Galli et al. 2012). We adopted the AD method (Chupina et al. 2001) in this paper for the studied Pismis clusters, which is based on searching for regularities at the locations of respective apices in the rectangular projection of the celestial sphere.

The available information in the literature for all studied Pismis clusters is as follows:

(a) Pismis 2: ($\alpha_{2000} = 8^{h}17^{m}54^{s}$, $\delta_{2000} = -41°40'00''$; $l = 258.°851$, $b = -3.°338$). Phelps et al. (1994) studied Pismis 2 for the first time in V and I filters. They estimated log(age) of the cluster as 9.04. Along with this, Janes & Phelps (1994) determined the value of $E(B-V)$ as 1.48 for this cluster. Dutra & Bica (2000) compared reddenings derived from maps by Miller et al. (1995) as 2.27 and from photometric methods as 1.48 and found reasonable agreement between the two at low Galactic latitudes except for some objects, and Pismis 2 was among them. They described this discrepancy due to dust clouds in the disk background of the clusters. Di Fabrizio et al. (2001) studied this cluster using CCD photometric data in *BVI* bands and found higher differential reddening of 0.04–0.06, and the value of interstellar reddening $E(B-V)$ ranges

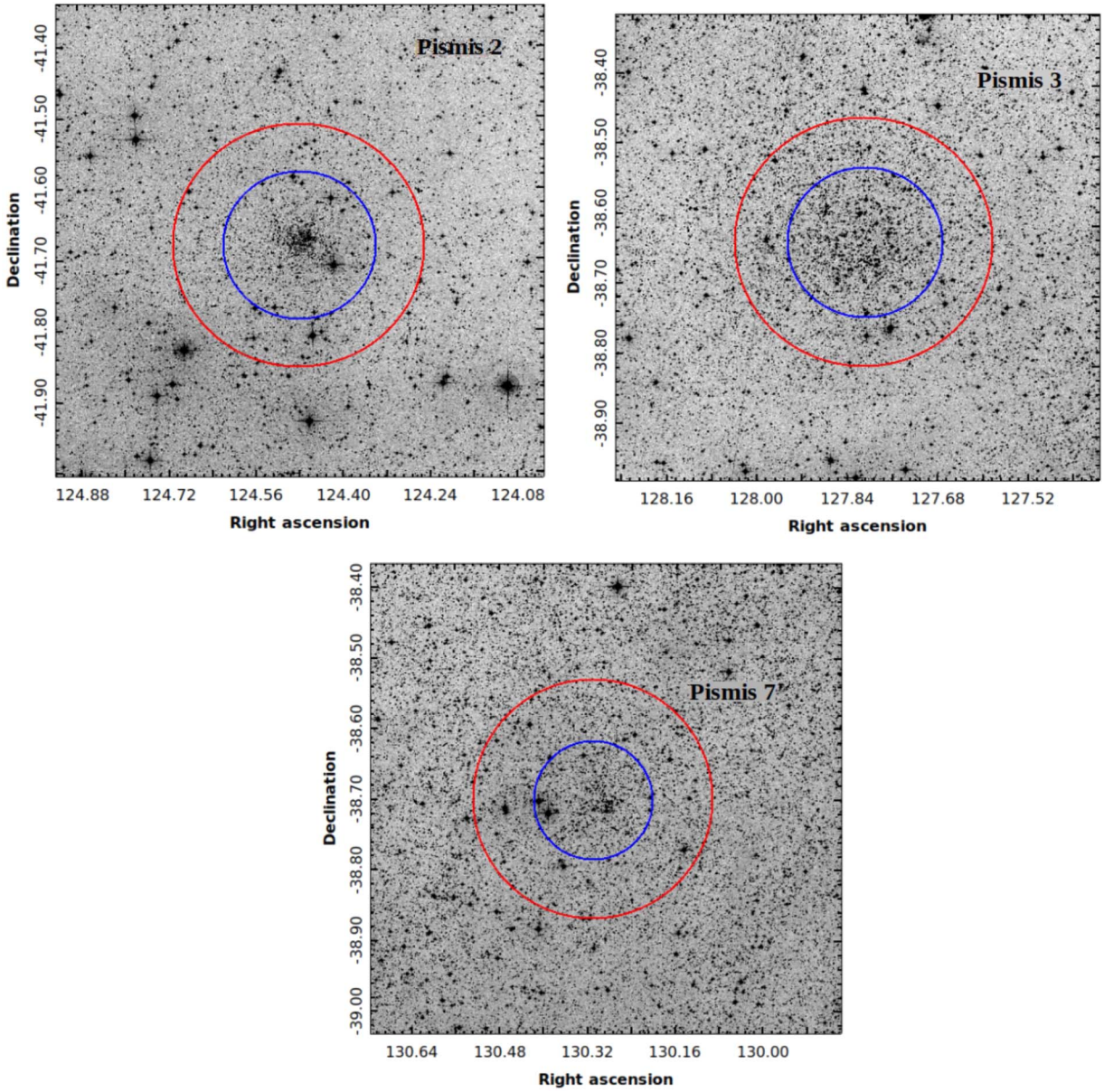

Figure 1. The finding chart of clusters Pi 2, Pi 3, and Pi 7 taken from the Leicester Database and Archive Service (LEDAS). The inner circle shows the cluster's radius (5.′5, 6.′5, and 4.′5 for clusters Pi 2, Pi 3, and Pi 7), and the outer ring denotes our data extraction radius of 10′ for all clusters.

between 1.26 and 1.32 toward the cluster. They also determined the log(age) of the cluster as 9.04–9.08 and distance modulus as 12.5–17.7 mag. Friel et al. (2002) calculated the mean [Fe/H] value of the cluster as −0.07 and corresponding Z value as 0.010.

(b) Pismis 3: ($\alpha_{2000} = 8^h31^m22^s$, $\delta_{2000} = -38°39'00''$; $l = 257.°865$, $b = 0.°502$). Janes (1988) calculated the cluster extent as 6.′5. Then, for the first time, Carraro & Ortolani (1994) studied this cluster in detail using CCD BV photometry. They found that Pismis 3 has log(age) ∼ 9.30, $E(B-V) = 1.35$, and distance ∼1.5 kpc and is a metal-poor cluster.

(c) Pismis 7: ($\alpha_{2000} = 8^h41^m08^s$, $\delta_{2000} = -38°42'00''$; $l = 259.°052$, $b = 1.°994$). This is a very poorly studied cluster. We found only two detailed studies about the cluster. Ahumada (2005) studied the cluster Pismis 7 using broadband optical CCD photometry and calculated cluster parameters such as $E(B-V) = 0.69$, log(age) = 8.7, and distance modulus = 13.46. Cakmak et al. (2021) studied this cluster using the Gaia DR2 data and calculated the Z value as 0.008 and log(age) of the cluster as 9.00. They also studied the dynamical evolution of the cluster and found that the outer part of this cluster expands with time.

(d) Pismis 12: ($\alpha_{2000} = 9^h20^m00^s$, $\delta_{2000} = -45°07'00''$; $l = 268.°640$, $b = 3.°216$). Pismis 12 is a very poor OC and was explored only by Bica & Bonatto (2011) in detail, using Two Micron All Sky Survey data. They calculated the distance of the cluster as 1.9 kpc, radius as 5.′5, and log(age) as 9.11.

(e) Pismis 15: ($\alpha_{2000} = 9^h34^m45^s$, $\delta_{2000} = -48°02'00''$; $l = 272.°493$, $b = 2.°869$). Pismis 15 is an intermediate-age OC. Carraro et al. (2005) studied Pismis 15 for the first time using BVI CCD photometry. They found that the log(age) of the cluster is 9.11, the metallicity Z value is ∼0.008,

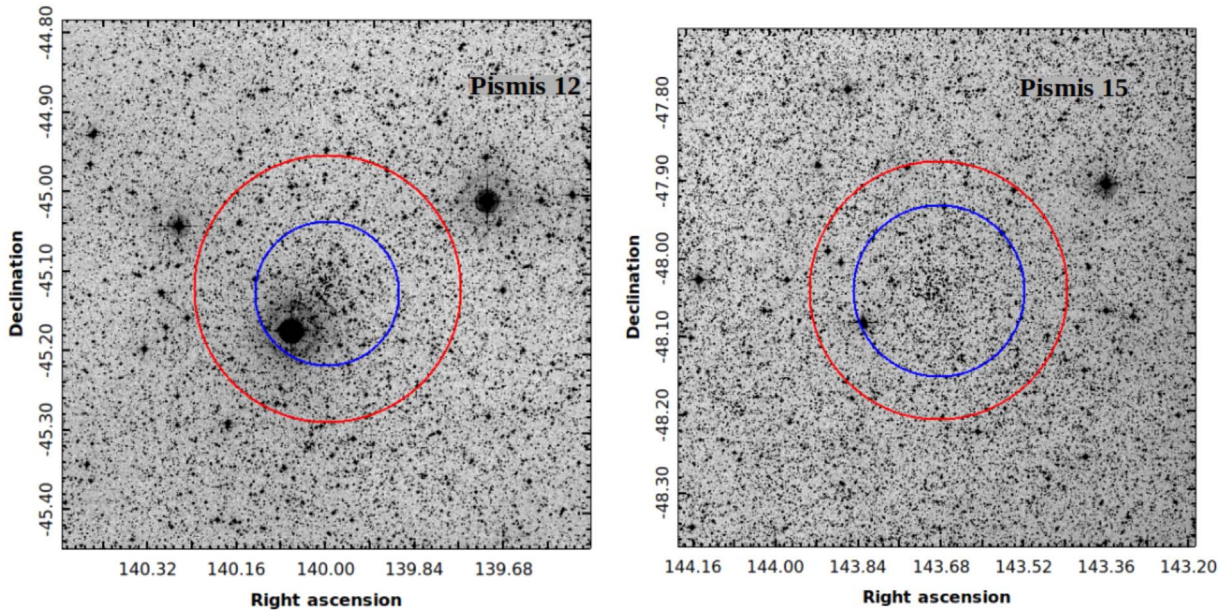

Figure 2. Same as Figure 1, but for clusters Pi 12 and Pi 15. The inner circle indicates the radius value as 5.′5 and 6.′5 for clusters Pi 12 and Pi 15, respectively.

$E(B-V) = 0.53$, and it is at a distance of 2.9 kpc.

The layout of the paper is as follows. A brief explanation of the data used is described in Section 2. Section 3 deals with investigating proper motion (PM), determination of the membership probability of stars, and identifying the blue straggler stars (BSSs). The structural properties and derivation of fundamental parameters using the most probable cluster members have been carried out in Section 4. Luminosity function (LF) and mass function (MF) are discussed in Section 5. Section 6 is devoted to the dynamics and kinematics of the clusters. We have addressed the orbit of clusters in Section 7. The conclusions are presented in Section 8.

2. Data

We have used a photometric and astrometric database for 10′-radius fields from the Gaia EDR3 (Gaia Collaboration et al. 2021) catalog for the Pismis clusters under study. The cluster finding charts are taken from the Digitized Sky Survey (DSS) and shown in Figures 1 and 2. The total number of stars within the applied radius was 6302, 8294, 8705, 9297, and 10,749 for clusters Pi 2, Pi 3, Pi 7, Pi 12, and Pi 15, respectively. The main quantities contained in the above catalog are positions (α, δ), parallaxes, and PMs ($\mu_\alpha \cos\delta$, μ_δ) up to a limiting magnitude of $G = 21$ mag. The uncertainties in the parallax values are ∼0.02–0.03 mas for sources at $G \leqslant 15$ mag and ∼0.07 mas for sources with $G \sim 17$ mag. The uncertainties in the corresponding PM components are ∼0.01–0.02 mas yr^{-1} (for $G \leqslant$ 15 mag), ∼0.05 mas yr^{-1} (for $G \sim 17$ mag), ∼0.4 mas yr^{-1} (for $G \sim 20$ mag), and ∼1.4 mas yr^{-1} (for $G \sim 21$ mag). In this paper, we have used stars up to 20th G mag.

3. Mean Proper Motion and Field Star Separation

The precise PMs from Gaia EDR3 are sufficient to provide an initial selection of members in a cluster. PMs play a prominent role in separating field stars from the main sequence (MS) and deriving accurate fundamental parameters (Yadav et al. 2013; Sariya et al. 2021; Bisht et al. 2022). To detect the distribution of cluster and field stars, PM components ($\mu_\alpha \cos\delta$, $\mu\delta$) have been plotted as vector point diagrams (VPDs) in the top panels of Figures 3 and 4. The bottom panels show all clusters' corresponding G versus ($G_{BP}-G_{RP}$) color–magnitude diagrams (CMDs). The left panel shows all the stars, while the middle and right panels show the probable cluster members and field region stars, respectively. A circle of 0.3, 0.6, 0.4, 0.4, and 0.3 mas yr^{-1} for clusters Pi 2, Pi 3, Pi 7, Pi 12, and Pi 15, respectively, around the distribution of cluster stars in the VPDs, characterizes our membership criteria. The selected radius in VPDs compromises losing cluster members with poor PMs and including field region stars (Sariya et al. 2018). The cluster's member stars are gravitationally bound, so they show a very narrow spread in parallaxes compared to field stars in parallax versus magnitude plots (Angelo et al. 2020). We calculated the weighted mean of parallax for stars inside the circle of the VPD having G mag brighter than 20 mag. In our selection method, we picked a star as the most probable member if it lies within the used radii in VPDs, having a PM error of $\leqslant$0.5 mas yr^{-1}, and having a parallax within 3σ from the mean parallax of the cluster. We have shown the CMDs of the most probable member in the lower middle panels in Figures 3 and 4. In this figure, the cluster's MS looks well defined for all studied clusters.

To estimate the mean PM, we consider cluster members as selected from VPDs and CMDs, as shown in Figures 3 and 4. We made the histograms for $\mu_\alpha \cos\delta$ and μ_δ as shown in Figures 5 and 6. The fitting of a Gaussian function to the histograms provides a mean PM in both the R.A. and decl. directions. We obtained PM values of (-4.723 ± 0.23 and 5.334 ± 0.24) mas yr^{-1}, (-4.776 ± 0.17 and 6.710 ± 0.19) mas yr^{-1}, (-3.204 ± 0.21 and 2.814 ± 0.24) mas yr^{-1}, (-6.707 ± 0.21 and 4.909 ± 0.20) mas yr^{-1}, and (-5.248 ± 0.25 and 3.432 ± 0.33) mas yr^{-1} for clusters Pi 2, Pi 3, Pi 7, Pi 12, and Pi 15, respectively. The above-estimated values of mean PMs for Pismis clusters fully agree with the values that are given by Cantat-Gaudin et al. (2020) and Liu & Pang (2019) as listed in Tables 1 and 2. Our derived values of mean PMs are more reliable than those of Dias et al. (2014) because our values are based on accurate Gaia EDR3 PM data.

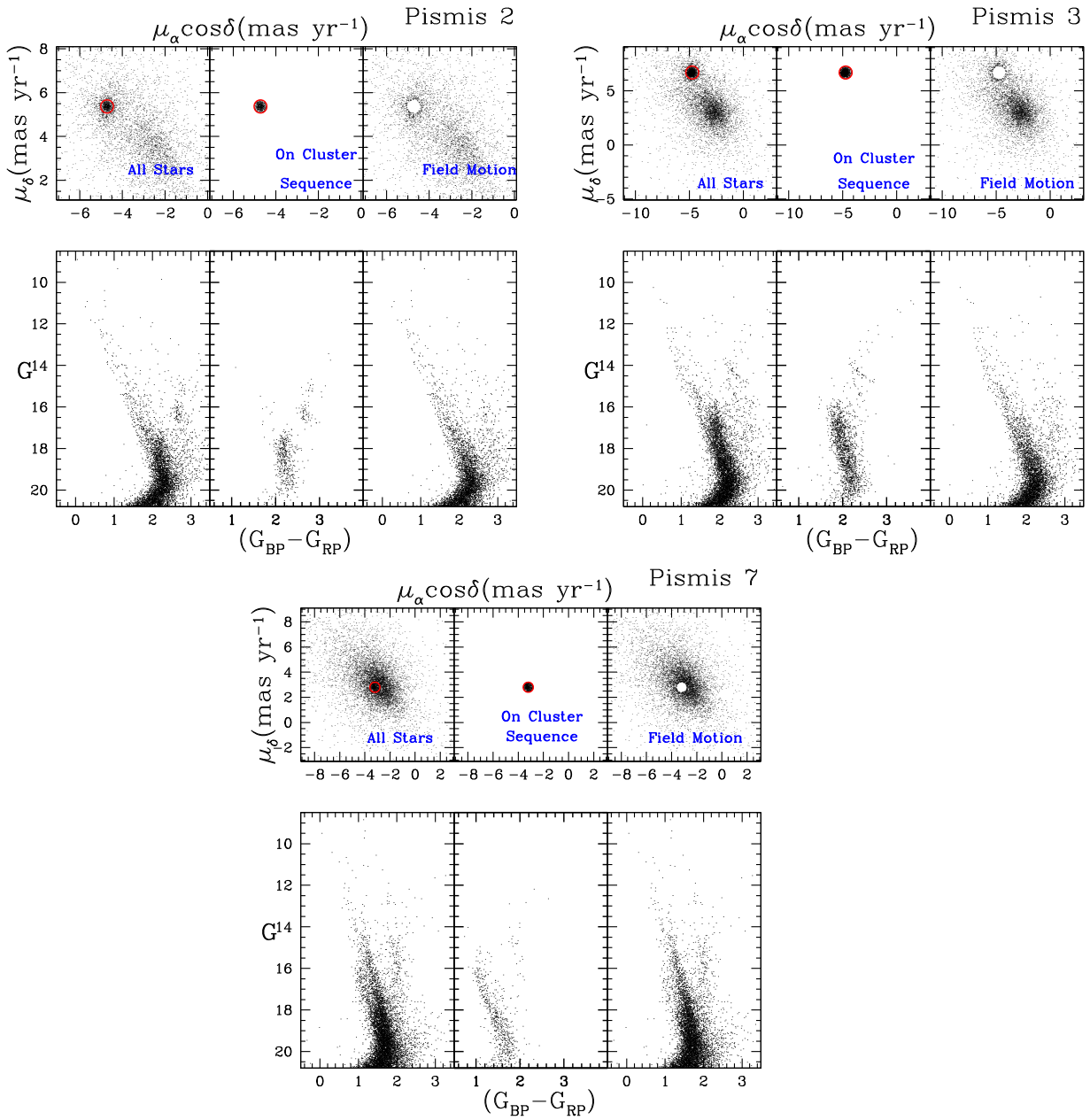

Figure 3. Top panels: PM VPD for clusters Pi 2, Pi 3, and Pi 7 based on Gaia EDR3. Bottom panels: G vs. $(G_{BP} - G_{RP})$ CMDs. Left: the entire sample. Middle: stars in VPDs within a circle of 0.3, 0.6, and 0.4 mas yr^{-1} of the cluster's mean for Pi 2, Pi 3, and Pi 7, respectively. Right: probable background/foreground field stars in the direction of these clusters. We have used only stars with PM σ smaller than 0.5 mas yr^{-1} in each coordinate.

3.1. Distance of Clusters Using Parallax

We used the star's parallax to acquire the distance of clusters Pi 2, Pi 3, Pi 7, Pi 12, and Pi 15. We have corrected the Gaia EDR3 parallax for these clusters after using the zero-point offset (−0.017 mas) given by Lindegren et al. (2020). We adopted the weighted mean method to find the mean value of parallax. The mean parallax is estimated as 0.23 ± 0.02 mas, 0.38 ± 0.03 mas, 0.17 ± 0.02 mas, 0.44 ± 0.01 mas, and 0.36 ± 0.01 mas for the clusters Pi 2, Pi 3, Pi 7, Pi 12, and Pi 15, respectively, and the corresponding distance values (reciprocal of cluster parallax) are 4.34 ± 0.2 kpc, 2.63 ± 0.3 kpc, 5.88 ± 0.3 kpc, 2.27 ± 0.2 kpc, and 2.70 ± 0.3 kpc. Our obtained value of mean parallax for all studied objects agrees with the value given by Liu & Pang (2019) and Cantat-Gaudin et al. (2018). We have also employed the method discussed by Bailer-Jones et al. (2018) for distance estimation from the parallax of a cluster. The correct approach is to acquire the distance values from the parallaxes of stars via probabilistic analysis, which includes a mixture of likelihood (measurements) and prior (assumption). Bailer-Jones (2015) investigated different types of priors, and Bailer-Jones et al. (2018) delivered an exponentially decreasing space density prior to distance r. The prior depends on a length scale parameter that can be obtained by fitting a three-dimensional model of the Galaxy observed by Gaia and varies smoothly as a function of Galactic longitude and latitude. With the help of the selected

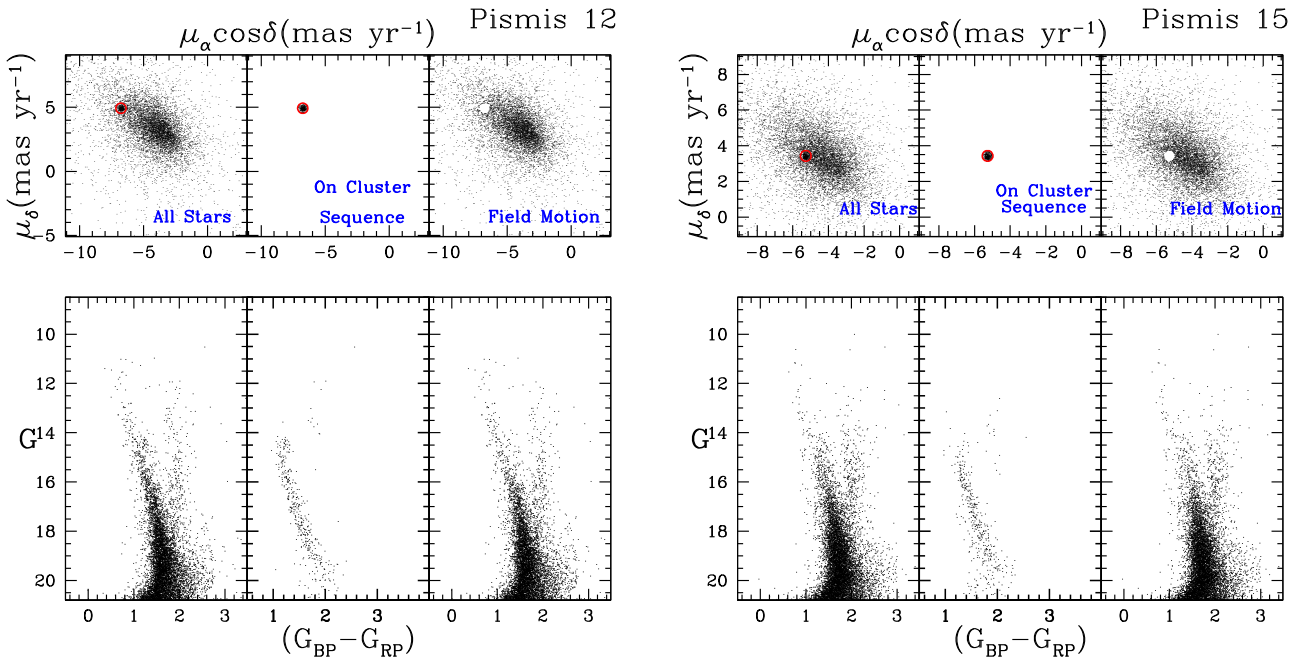

Figure 4. Same as Figure 3, but for clusters Pi 12 and Pi 15. The radii of circles for both clusters are 0.4 and 0.3 mas yr^{-1}.

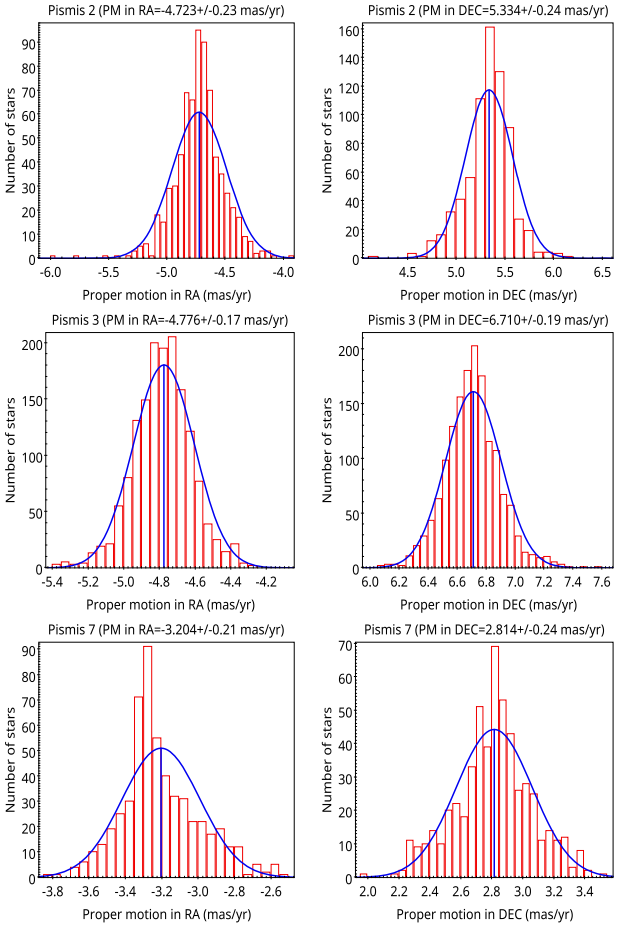

Figure 5. PM histograms of 0.1 mas yr^{-1} bins in R.A. and decl. of the clusters Pi 2, Pi 3, and Pi 7. The Gaussian function fit to the central bins provides the mean values in both directions as shown in each panel.

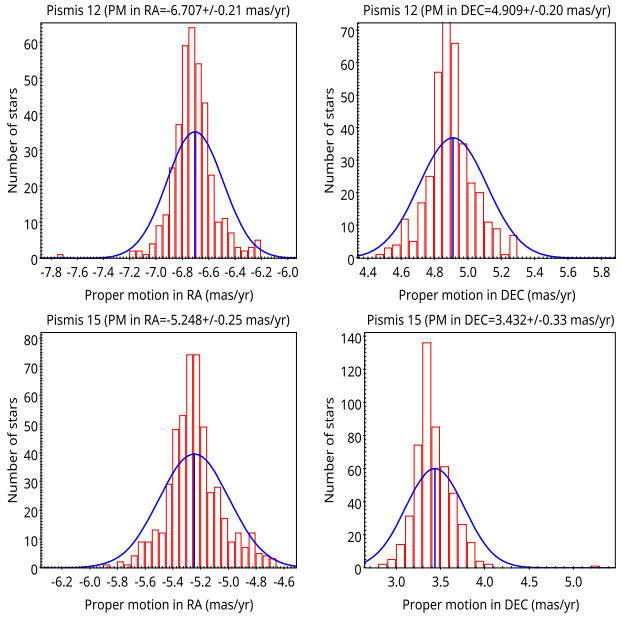

Figure 6. Same as Figure 5, but for clusters Pi 12 and Pi 15.

prior, the distance of an object can be calculated using a posterior, which is a probability of a known value (parallax) given an unknown value (distance). This technique gives objects a pure geometric distance independent of interstellar extinction's physical properties toward an individual star. Finally, our obtained values are 4.50 ± 0.4 kpc, 2.67 ± 0.3 kpc, 5.10 ± 0.4 kpc, 2.15 ± 0.4 kpc, and 2.50 ± 0.3 kpc for Pi 2, Pi 3, Pi 7, Pi 12, and Pi 15, respectively. Our obtained values agree with the values 4.066, 2.349, 4.611, 2.107, and 2.559 kpc for clusters Pi 2, Pi 3, Pi 7, Pi 12, and Pi 15, respectively, as given by Cantat-Gaudin et al. (2020).

These values of cluster distance are in reasonable agreement with the values 4.76 ± 0.6 kpc, 2.79 ± 0.30 kpc, 5.18 ± 0.30 kpc, 1.98 ± 0.40 kpc, and 2.22 ± 0.50 kpc for clusters Pi 2, Pi 3, Pi 7, Pi 12, and Pi 15, respectively, as acquired from the isochrone fitting method. The distances computed using the

Table 1
Comparison of Our Obtained Fundamental Parameters for Clusters Pismis 2, Pismis 3, and Pismis 7 with the Literature values

Parameters	Pismis 2	Pismis 3	Pismis 7	Reference
(R.A., decl.) (deg)	(124.483 ± 0.06, −41.674 ± 0.04)	(127.826 ± 0.09, −38.650 ± 0.07)	(130.293 ± 0.08, −38.701 ± 0.06)	Present study
	(124.477, −41.674)	(127.834, −38.640)	(130.287, −38.699)	Cantat-Gaudin et al. (2020)
	(124.482, −41.676)	(127.837, −38.636)	(130.274, −38.687)	Liu & Pang (2019)
	(127.475, −41.660)	(127.84, −38.65)	(130.283, −38.700)	Sampedro et al. (2017)
	(124.48, 41.666)	(127.809, −38.654)	(130.295, −38.704)	Kharchenko et al. (2016)
	(124.475, −41.666)	(127.841, −38.650)	⋯	Dias et al. (2014)
Cluster radius (arcmin)	5.5	6.5	4.5	Present study
	3.0	3.5	⋯	Dias et al. (2014)
($\mu_\alpha \cos(\delta)$, μ_δ) (mas yr^{-1})	(−4.723 ± 0.23, 5.33 ± 0.24)	(−4.776 ± 0.17, 6.711 ± 0.19)	(−3.204 ± 0.21, 2.814 ± 0.24)	Present study
	(−4.756, 5.325)	(−4.809, 6.645)	(−3.312, 2.793)	Cantat-Gaudin et al. (2020)
	(−4.728, 5.300)	(−4.793, 6.636)	(−3.22, 2.824)	Liu & Pang (2019)
	(−5.72, 0.89)	(−3.42, 3.82)	⋯	Dias et al. (2014)
Age (log)	9.30	9.05	8.95	Present study
	8.93	9.47	8.64	Liu & Pang (2019)
	9.06	9.03	8.70	Sampedro et al. (2017)
	9.05	8.92	8.70	Kharchenko et al. (2016)
	9.04–9.08	⋯	⋯	Di Fabrizio et al. (2001)
	9.04	⋯	⋯	Phelps et al. (1994)
	⋯	9.30	⋯	Carraro & Ortolani (1994)
	⋯	⋯	8.7	Ahumada (2005)
	⋯	⋯	9.0	Cakmak et al. (2021)
Parallax (mas)	0.23 ± 0.02	0.38 ± 0.03	0.17 ± 0.02	Present study
	0.221	0.403	0.150	Cantat-Gaudin et al. (2020)
	0.267	0.413	0.223	Liu & Pang (2019)
Distance modulus (mag)	15.30 ± 0.6	14.20 ± 0.7	14.80 ± 0.5	Present study
	12.5–17.7	⋯	⋯	Di Fabrizio et al. (2001)
	⋯	⋯	13.46	Ahumada (2005)
Distance (kpc)	4.50 ± 0.4	2.67 ± 0.3	5.10 ± 0.4	Present study
	4.00	2.316	5.57	Cantat-Gaudin et al. (2020)
	3.31	1.394	4.90	Sampedro et al. (2017)
	2.754	1.418	4.783	Kharchenko et al. (2016)
	⋯	1.5	⋯	Carraro & Ortolani (1994)
(X, Y, Z) (kpc)	(−0.84, −4.25, −0.25)	(−0.55, −2.57, 0.02)	(−1.08, −5.59, 0.20)	Present study
	(−0.77, −3.92, −0.23)	(−0.48, −2.26, 0.02)	(−1.06, −5.46, 0.19)	Cantat-Gaudin et al. (2020)

trigonometric parallaxes are more factual than the other techniques because this method is not conditional on the object's intrinsic properties. As Bailer-Jones (2015) discussed, the parallax data from Gaia have corresponding error values, affecting the result if we calculate distances by directly inverting the parallax values.

3.2. Membership Probabilities

It is required to separate field stars from the cluster member stars to estimate the physical and dynamical parameters of the clusters (e.g., Dias et al. 2018a, 2018b; Sariya et al. 2018; Bisht et al. 2021b; Sariya et al. 2021; Bisht et al. 2021a, 2022). We have adopted the approach given by Balaguer-Núñez et al. (1998) by using the PM database from the Gaia EDR3 catalog to determine the membership of stars in Pismis clusters. This method uses two frequency distribution functions for a particular ith star. The frequency distributions of cluster members (ϕ_c^ν) and field stars (ϕ_f^ν) are presented by the equations given below:

$$\phi_c^\nu = \frac{1}{2\pi\sqrt{(\sigma_c^2+\epsilon_{xi}^2)(\sigma_c^2+\epsilon_{yi}^2)}} \times \exp\left\{-\frac{1}{2}\left[\frac{(\mu_{xi}-\mu_{xc})^2}{\sigma_c^2+\epsilon_{xi}^2}+\frac{(\mu_{yi}-\mu_{yc})^2}{\sigma_c^2+\epsilon_{yi}^2}\right]\right\} \quad (1)$$

Table 2
Same as Table 1, but for Clusters Pismis 12 and Pismis 15

Parameters	Pismis 12	Pismis 15	Reference
(R.A., decl.) (deg)	(140.008 ± 0.08, −45.128 ± 0.05)	(143.688 ± 0.10, −48.043 ± 0.06)	Present study
	(140.007, −45.131)	(143.684, −48.04)	Cantat-Gaudin et al. (2020)
	(140.028, −45.1298)	(143.678, −48.0451)	Liu & Pang (2019)
	(140.00, −45.116)	(143.687, −48.033)	Sampedro et al. (2017)
	(139.994, −45.107)	(143.683, −48.026)	Kharchenko et al. (2016)
	(140.00, −45.116)	(143.687, −48.03)	Dias et al. (2014)
Cluster radius (arcmin)	5.5	6.5	Present study
	3.5	2.8	Dias et al. (2014)
($\mu_\alpha \cos(\delta)$, μ_δ) (mas yr^{-1})	(−6.707 ± 0.21, 4.909 ± 0.20)	(−5.248 ± 0.25, 3.432 ± 0.33)	Present study
	(−6.748, 4.833)	(−5.302, 3.329)	Cantat-Gaudin et al. (2020)
	(−6.675, 4.815)	(−5.316, 3.357)	Liu & Pang (2019)
	(−4.40, 1.65)	(−4.67, 4.90)	Dias et al. (2014)
Age (log)	9.40	9.15	Present study
	9.32	9.01	Liu & Pang (2019)
	9.40	9.11	Sampedro et al. (2017)
	9.20	9.09	Kharchenko et al. (2016)
	9.11	⋯	Bica & Bonatto (2011)
	⋯	9.11	Carraro et al. (2005)
Parallax (mas)	0.44 ± 0.01	0.36 ± 0.01	Present study
	0.431	0.354	Cantat-Gaudin et al. (2020)
	0.444	0.359	Liu & Pang (2019)
Distance modulus (mag)	12.70 ± 0.6	13.20 ± 0.5	Present study
Distance (kpc)	2.15 ± 0.4	2.50 ± 0.3	Present study
	2.17	2.61	Cantat-Gaudin et al. (2020)
	1.714	2.90	Sampedro et al. (2017)
	2.221	2.558	Kharchenko et al. (2016)
	1.9	⋯	Bica & Bonatto (2011)
	⋯	2.9	Carraro et al. (2005)
(X, Y, Z) (kpc)	(−0.05, −2.26, 0.13)	(0.12, −2.69, 0.13)	Present study
	(−0.05, −2.17, 0.12)	(0.11, −2.60, 0.13)	Cantat-Gaudin et al. (2020)

and

$$\phi_f^{\nu} = \frac{1}{2\pi\sqrt{(1-\gamma^2)}\sqrt{(\sigma_{xf}^2+\epsilon_{xi}^2)(\sigma_{yf}^2+\epsilon_{yi}^2)}} \times \exp\left\{-\frac{1}{2(1-\gamma^2)}\left[\frac{(\mu_{xi}-\mu_{xf})^2}{\sigma_{xf}^2+\epsilon_{xi}^2} - \frac{2\gamma(\mu_{xi}-\mu_{xf})(\mu_{yi}-\mu_{yf})}{\sqrt{(\sigma_{xf}^2+\epsilon_{xi}^2)(\sigma_{yf}^2+\epsilon_{yi}^2)}} + \frac{(\mu_{yi}-\mu_{yf})^2}{\sigma_{yf}^2+\epsilon_{yi}^2}\right]\right\}, \quad (2)$$

where (μ_{xi}, μ_{yi}) are the PMs of the ith star, although (ϵ_{xi}, ϵ_{yi}) are corresponding errors in PMs. (μ_{xc}, μ_{yc}) represent the cluster's PM center, and (μ_{xf}, μ_{yf}) are PM center coordinates for field stars. The intrinsic PM dispersion is denoted by σ_c for members, whereas σ_{xf} and σ_{yf} show the field intrinsic PM dispersions. The correlation coefficient γ is calculated as

$$\gamma = \frac{(\mu_{xi}-\mu_{xf})(\mu_{yi}-\mu_{yf})}{\sigma_{xf}\,\sigma_{yf}}. \quad (3)$$

A tight bunch of stars are found at (−4.723, 5.334) mas yr^{-1}, (−4.776, 6.710) mas yr^{-1}, (−3.204, 2.814) mas yr^{-1}, (−6.707, 4.909) mas yr^{-1}, and (−5.248, 3.432) mas yr^{-1} and in circular regions having radii of 0.3, 0.6, 0.4, 0.4, and 0.3 mas yr^{-1} for clusters Pi 2, Pi 3, Pi 7, Pi 12, and Pi 15, respectively. Assuming a distance of 4.50, 2.67, 5.60, 2.15, and 2.50 kpc and radial velocity dispersion of 1 km s^{-1} for open star clusters (Girard et al. 1989), the expected dispersion (σ_c) in PMs would be 0.05, 0.09, 0.04, 0.09, and 0.07 mas yr^{-1} for clusters Pi 2, Pi 3, Pi 7, Pi 12, and Pi 15, respectively. For field region stars, we have estimated (μ_{xf}, μ_{yf}) = (−2.8, 4.0) mas yr^{-1} and (σ_{xf}, σ_{yf}) = (2.6, 3.8) mas yr^{-1} for Pi 2, (μ_{xf}, μ_{yf}) = (−3.0, 3.5) mas yr^{-1} and (σ_{xf}, σ_{yf}) = (1.8, 1.5) mas yr^{-1} for Pi 3, (μ_{xf}, μ_{yf}) = (−3.5, 3.9) mas yr^{-1} and (σ_{xf}, σ_{yf}) = (2.6, 3.2) mas yr^{-1} for Pi 7, (μ_{xf}, μ_{yf}) = (−4.8, 3.5) mas yr^{-1} and (σ_{xf}, σ_{yf}) = (2.2, 1.6) mas yr^{-1} for Pi 12, and (μ_{xf}, μ_{yf}) = (−4.9, 4.2) mas yr^{-1} and (σ_{xf}, σ_{yf}) = (1.9, 2.3) mas yr^{-1} for Pi 15.

Considering n_c and n_f as the normalized number of cluster and field stars, respectively (i.e., $n_c + n_f = 1$), the absolute distribution function can be computed as

$$\phi = (n_c \times \phi_c^{\nu}) + (n_f \times \phi_f^{\nu}). \quad (4)$$

Finally, the membership probability of the ith star is given by

$$P_\mu(i) = \frac{\phi_c(i)}{\phi(i)}. \quad (5)$$

From this analysis, we identified 635, 1488, 535, 368, and 494 stars as cluster members for clusters Pi 2, Pi 3 , Pi 7, Pi 12, and Pi 15, respectively, with membership probability higher than 90% and $G \leqslant 20$ mag. In Figure 7, we plotted membership probability versus G magnitude. In this figure, cluster members and field stars are separated out. The most probable cluster members with high membership probability ($\geqslant$90%) are shown by red circles in Figure 7.

BSSs are among the numerous massive stars in a cluster. The BSSs are fascinating objects present in stellar atmospheres like the clusters (Johnson & Sandage 1955; Sandage 1962; Ahumada & Lapasset 1995). BSSs are the most massive stars in a cluster formed via binary or higher-order stellar interactions. BSSs are

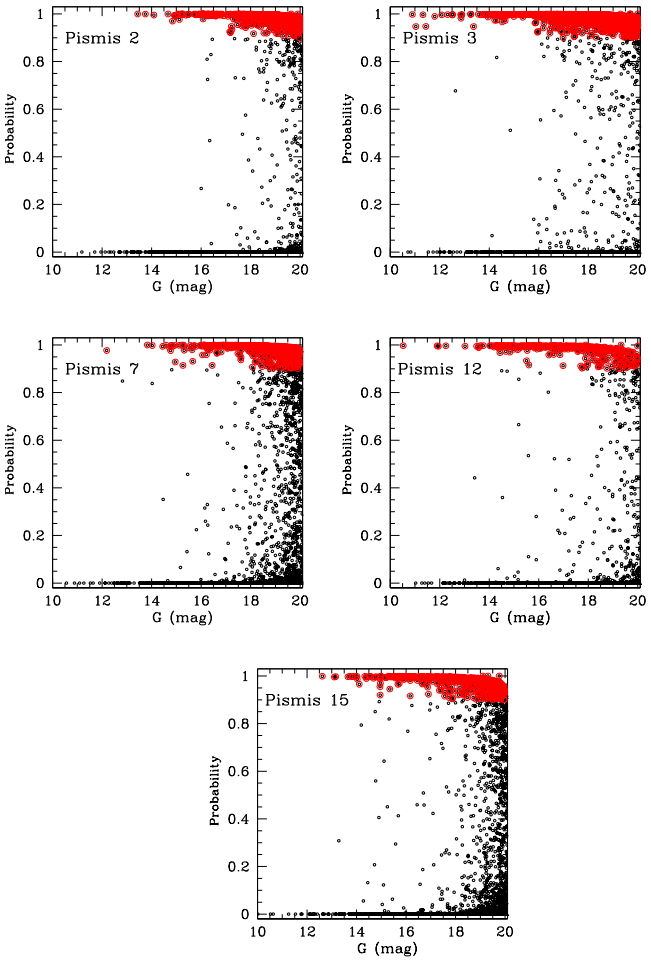

Figure 7. Membership probability as a function of G magnitude. The red circles show the cluster members with a membership probability higher than 90% in all panels.

stars lying above the MS turnoff region in CMDs. This paper found five- and two-member BSSs in clusters Pi 2 and Pi 15, respectively, located at a radial distance of 0.′74–1.′78 and 2.′71–3.′29. Our investigation firmly suggests that the determined BSSs are confirmed cluster members with a membership probability higher than 90%. We have shown all identified BSSs in contour plots for Pi 2 and Pi 15 as shown in Figure 8 with blue filled circles, while the red filled circle is the cluster center.

4. Structural Properties of Pismis Clusters

4.1. Spatial Structure: Radial Density Profile

Accurate information of the central coordinates of a cluster is essential for a reliable estimation of the cluster's fundamental parameters, such as age, distance, reddening, etc. We have applied the star-count method to calculate the central coordinates of the Pismis clusters under study. The resulting histograms in both the R.A. and decl. directions are shown in Figures 9 and 10. The Gaussian curve fitting is applied to the central regions in the histograms. The fitting provides the central coordinates as $\alpha = 124.483 \pm 0.06$ deg ($8^{h}17^{m}55.^{s}9$) and $\delta = -41.674 \pm 0.04$ deg ($-41°40'26.''4$) for Pi 2, $\alpha = 127.826 \pm 0.09$ deg ($8^{h}31^{m}18.^{s}2$) and $\delta = -38.650 \pm 0.07$ deg ($-38°39'00''$) for Pi 3, $\alpha = 130.293 \pm 0.08$ deg ($8^{h}41^{m}10.^{s}3$) and $\delta = -38.701 \pm 0.06$ deg ($-38°42'3.''6$) for Pi 7, $\alpha = 140.008 \pm 0.08$ deg ($9^{h}20^{m}1.^{s}9$) and $\delta = -45.128 \pm 0.05$ deg ($-45°7'40.''8$) for Pi 12, and $\alpha = 143.688 \pm 0.10$ deg ($9^{h}34^{m}45.^{s}1$) and $\delta = -48.043 \pm 0.06$ deg ($-48°2'34.''8$)for Pi 15. These values of the cluster center are in agreement with the values given by Dias et al. (2014) and Cantat-Gaudin et al. (2020) as listed in Tables 1 and 2 for all clusters.

To understand the extent of the Pismis clusters, we have plotted the radial density profiles (RDPs) as shown in Figure 11 using the derived central coordinates in the above paragraph of this section. We divided the observed area of all clusters into many concentric rings around the cluster center. The number density, R_i, in the ith zone is determined by using the formula $R_i = \frac{N_i}{A_i}$, where N_i is the number of stars and A_i is the area of the ith zone. This RDP flattens at $r \sim 5.5$, 6.5, 4.5, 5.5, and 6.′5 for clusters Pi 2, Pi 3, Pi 7, Pi 12, and Pi 15, respectively, and begins to merge with the background density as shown in Figure 11. Thus, we consider these values as the cluster radius of respective clusters. A smooth solid line represents the fitted King (1962) profile:

$$f(r) = f_{\rm bg} + \frac{f_0}{1 + (r/r_c)^2}, \tag{6}$$

where r_c, f_0, and $f_{\rm bg}$ are the core radius, central density, and background density level, respectively. The background density level with errors is also shown by the dotted lines. By fitting the King model to RDPs, we estimated the structural parameters for all studied clusters in this analysis. The above-obtained parameters are listed in Table 3.

4.2. Tidal Radius

Tidal interactions are crucial to understanding the clusters' initial structure and dynamical evolution (Chumak et al. 2010). The tidal radius is the distance from the cluster center where gravitational acceleration caused by the cluster becomes equal to the tidal acceleration due to the parent Galaxy (von Hoerner 1957). The Galactic mass M_G inside a Galactocentric radius R_G is given by (Genzel & Townes 1987)

$$M_G = 2 \times 10^8 M_{\odot} \left(\frac{R_G}{30 \text{ pc}}\right)^{1.2}. \tag{7}$$

Estimated values of Galactic mass inside the Galactocentric radius (see Section 4.5) are found to be 1.4×10^{11} $M_{\odot}$. Kim et al. (2000) have introduced the formula for tidal radius R_t of clusters as

$$R_t = \left(\frac{M_c}{2M_G}\right)^{1/3} \times R_G, \tag{8}$$

where R_t and M_c indicate the cluster's tidal radius and total mass (see Section 5), respectively. The estimated values of tidal radius are 14.34 ± 0.8 pc, 17.57 ± 1.4 pc, 14.96 ± 0.9 pc, 11.35 ± 0.8 pc, and 12.68 ± 0.6 pc for clusters Pi 2, Pi 3, Pi 7, Pi 12, and Pi 15, respectively.

4.3. Age and Distance to the Clusters

To trace the Galactic structure and chemical evolution using OCs, the distance and age of OCs play the most significant role (Friel & Janes 1993). The CMDs of the clusters have been a convenient tool for identifying the member stars and estimating the fundamental cluster parameters. We have calculated the mean value of A_G (total extinction in the G band) for the

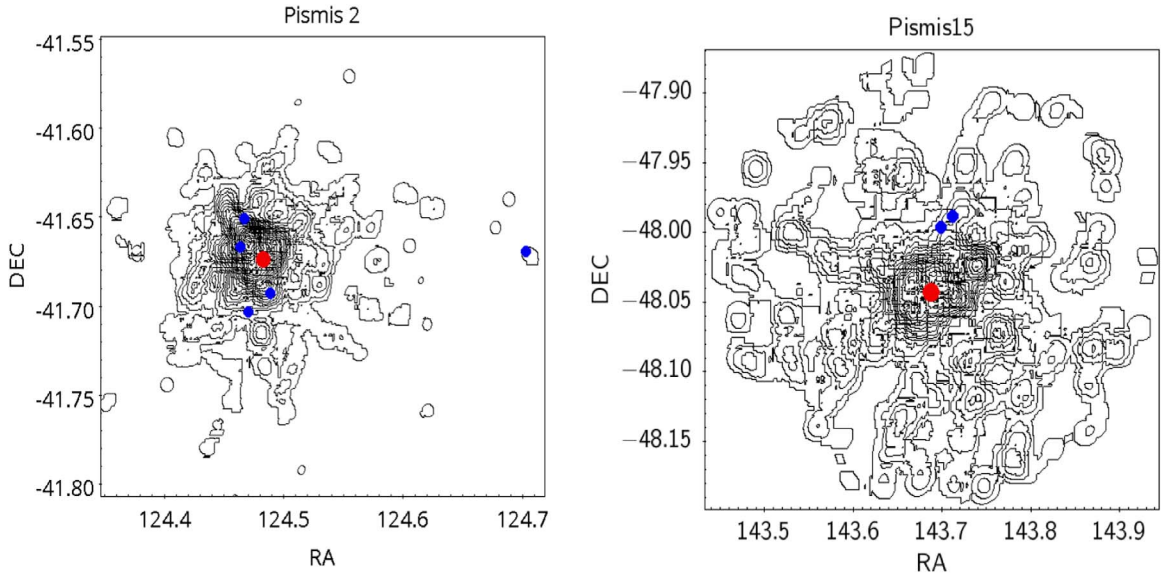

Figure 8. The contour plots to show the distribution of BSSs in clusters Pi 2 and Pi 15. Blue circles are BSSs, while the red circle indicates the cluster center.

studied clusters using the most probable members from Gaia DR2. Our obtained values of A_G are 1.91 ± 0.8, 2.00 ± 0.7, 1.23 ± 0.6, 1.22 ± 0.6, and 1.47 ± 0.5 for clusters Pi 2, Pi 3, Pi 7, Pi 12, and Pi 15, respectively, by adopting the weighted mean method. The main fundamental parameters (age, distance, and reddening) are estimated by fitting the theoretical isochrones to all the CMDs given by Marigo et al. (2017), as shown in Figure 12. We have used the isochrones of (log (age) = 9.25, 9.30, and 9.35) for Pi 2, (log(age) = 9.00, 9.05, and 9.10) for Pi 3, (log(age) = 8.90, 8.95, and 9.00) for Pi 7, (log(age) = 9.35, 9.40, and 9.45) for Pi 12, and (log (age) = 9.10, 9.15, and 9.20) for Pi 15. We used metallicity values of 0.008, 0.019, 0.008, 0.019, and 0.008 for clusters Pi 2, Pi 3, Pi 7, Pi 12, and Pi 15, respectively. Our used values of metallicity are in good agreement with Friel et al. (2002; $Z = 0.010$), Cakmak et al. (2021; $Z = 0.008$), and Carraro et al. (2005; $Z = 0.008$) for clusters Pi 2, Pi 7, and Pi 15, respectively. A satisfactory fitting of isochrones provides an age of 2.0 ± 0.22 Gyr, 1.1 ± 0.12 Gyr, 0.9 ± 0.10 Gyr, 2.5 ± 0.30 Gyr, and 1.4 ± 0.19 Gyr for clusters Pi 2, Pi 3, Pi 7, Pi 12, and Pi 15, respectively. Our obtained values of ages for Pismis clusters are in fair agreement with the values obtained by Sampedro et al. (2017) and are listed in Tables 1 and 2. The apparent distance modulus ($(m - M) = 15.30 \pm 0.6$ mag, 14.20 ± 0.7 mag, 14.80 ± 0.5 mag, 12.70 ± 0.6 mag, and 13.20 ± 0.5 mag for all Pismis clusters) provides a distance 4.76 ± 0.60 kpc, 2.79 ± 0.30 kpc, 5.18 ± 0.30 kpc, 1.98 ± 0.40 kpc, and 2.22 ± 0.50 kpc from the Sun for Pi 2, Pi 3, Pi 7, Pi 12, and Pi 15, respectively. The estimated distances for all clusters are in good agreement with the values given by Cantat-Gaudin et al. (2020), which are listed in Section 3.1, and Tables 1 and 2.

Several fundamental parameters (center, radius, age, distance, etc.) for these Pismis clusters have been derived by authors in the literature. Tables 1 and 2 present a comparison of our estimated parameters in this paper with previously published values. All the derived parameter values are comparable with the literature.

The Galactocentric coordinates of the clusters X (directed toward the Galactic center in the Galactic disk), Y (directed toward the Galactic rotation), and distance from the Galactic plane Z (directed toward the Galactic north pole) can be estimated using clusters' distances, longitude, and latitude. The Galactocentric distance has been estimated by considering 8.3 kpc (Bajkova & Bobylev 2016) as the distance of the Sun to the Galactic center. The above-obtained parameters for all clusters under study are listed in Tables 1 and 2.

5. Luminosity Function and Mass Function

LF and MF are associated with a well-known mass–luminosity relationship. In recent years, LFs and MFs have been determined for several OCs using CCD data and reliable cluster membership criteria (see Sagar et al. 1988; Kjeldsen & Frandsen 1991; Phelps & Janes 1993; Massey et al. 1995; Durgapal & Pandey 2001; Pandey et al. 2007; Bisht et al. 2019). We used a G versus ($G_{BP}-G_{RP}$) CMD to construct the LF for the clusters. For the LF, we first converted the apparent G magnitudes of the clusters' stars into absolute magnitudes considering the distance modulus of clusters. The constructed histograms in Figure 13 show the LFs of the Pismis clusters under study. We found that the LF of all the clusters increases on going toward the fainter stars except Pi 3, for which the LF starts decreasing after $\sim$3.5 M_G.

We should have precise information on clusters' IMF to understand the star formation events. Salpeter (1955) had determined the IMF for massive stars (higher than 1 $M_\odot$). According to Salpeter's power law, the number of stars in each mass range descreases with increasing mass. This paper uses the theoretical isochrones of Marigo et al. (2017) to convert the LF into the MF. The resulting MF is shown in Figure 14. The MF slope can be derived by using the following relation:

$$\log \frac{dN}{dM} = -(1 + x)\log(M) + \text{constant}. \quad (9)$$

In the above power-law equation, dN represents the number of stars in a mass bin dM with central mass M, and x is the MF slope. The MF slopes are found to be 0.27 ± 0.16, 0.86 ± 0.27, 1.08 ± 0.32, 0.89 ± 0.38, and 1.07 ± 0.28 for clusters Pi 2, Pi 3, Pi 7, Pi 12, and Pi 15, respectively. The acquired slopes for

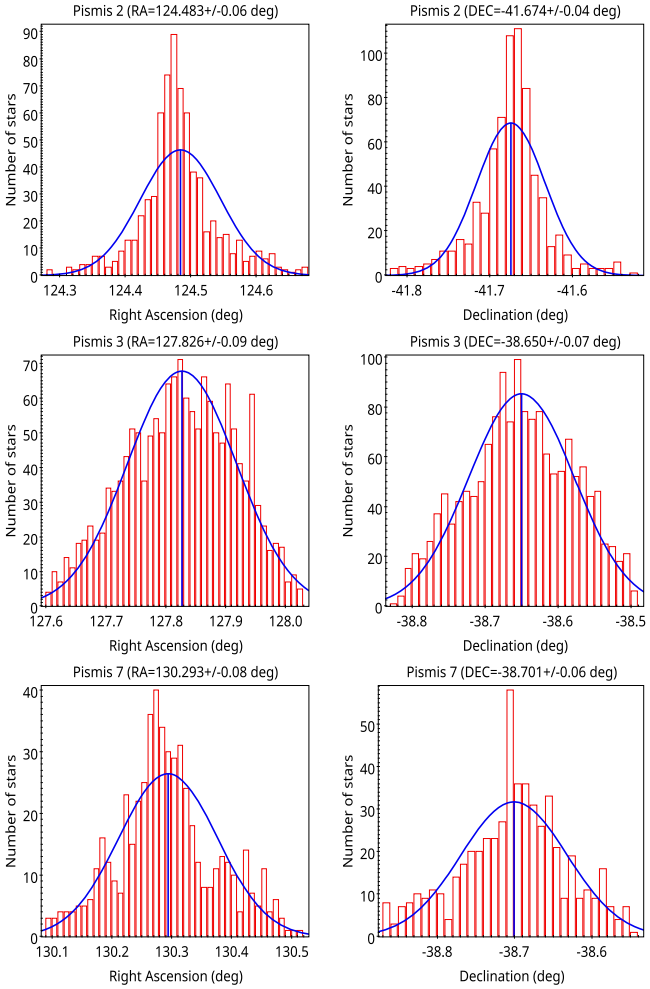

Figure 9. Profiles of stellar counts across the region of clusters Pi 2, Pi 3, and Pi 7. The Gaussian fits have been applied. The center of symmetry about the peaks of R.A. and decl. is taken to be the position of the cluster's center.

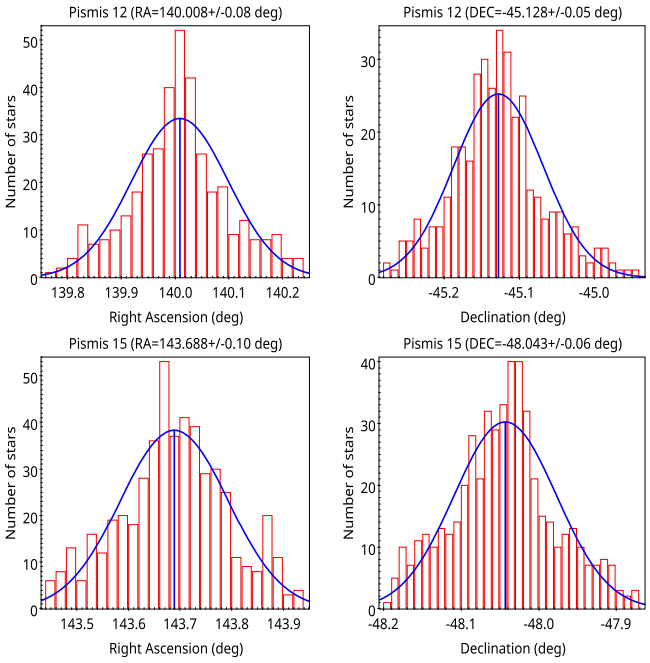

Figure 10. Same as Figure 9, but for clusters Pi 12 and Pi 15.

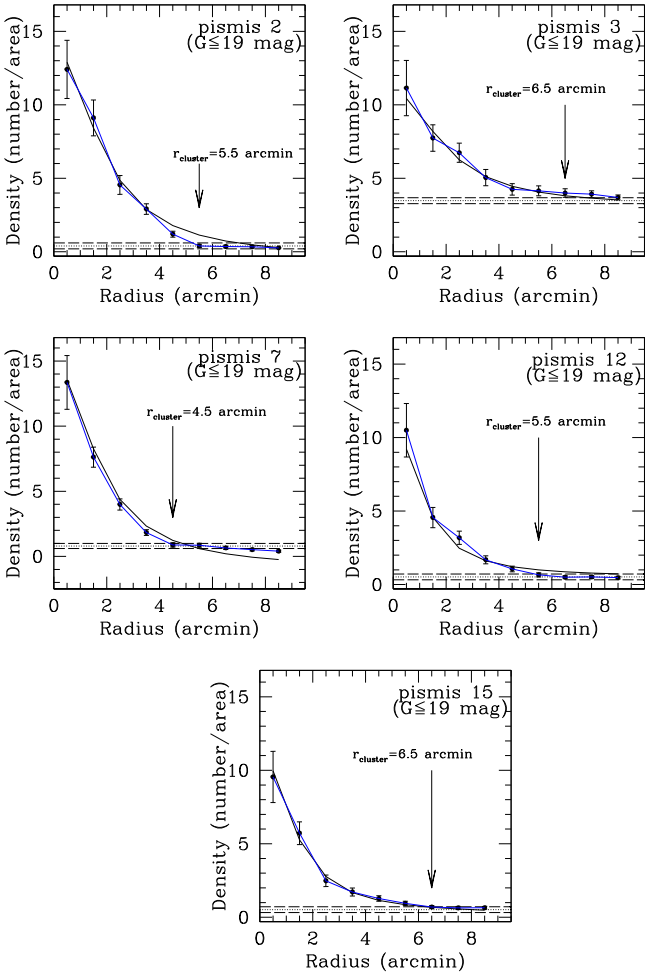

Figure 11. Surface density distribution of the Pismis clusters under study. Errors are determined from sampling statistics ($=\frac{1}{\sqrt{N}}$, where N is the number of cluster members used in the density estimation at that point). The smooth line represents the fitted profile of King (1962), whereas the dotted line shows the background density level. Long dashed lines represent the errors in background density.

all the clusters are flatter than the Salpeter value, suggesting a possibility of dynamical evolution in the studied clusters. We have estimated the total mass for all Pismis clusters under study, considering the derived MF slopes within the respective mass ranges. All derived MF parameters are listed in Table 4.

6. Dynamical and Kinematical Analysis

6.1. Dynamical Relaxation Time of Clusters

In the lifetime of star clusters, encounters between its member stars gradually lead to increased energy equipartition throughout the clusters. The timescale on which a cluster will lose all traces of its initial conditions is well represented by its relaxation time T_R, which is given by

$$T_R = \frac{8.9 \times 10^5 \sqrt{N} \times R_h^{3/2}}{\sqrt{m} \times \log(0.4N)}. \quad (10)$$

In the above formula, N denotes the cluster members, R_h is the radius within which half of the cluster mass is accommodated, and m is the mean mass of the cluster stars (Spitzer & Hart 1971).

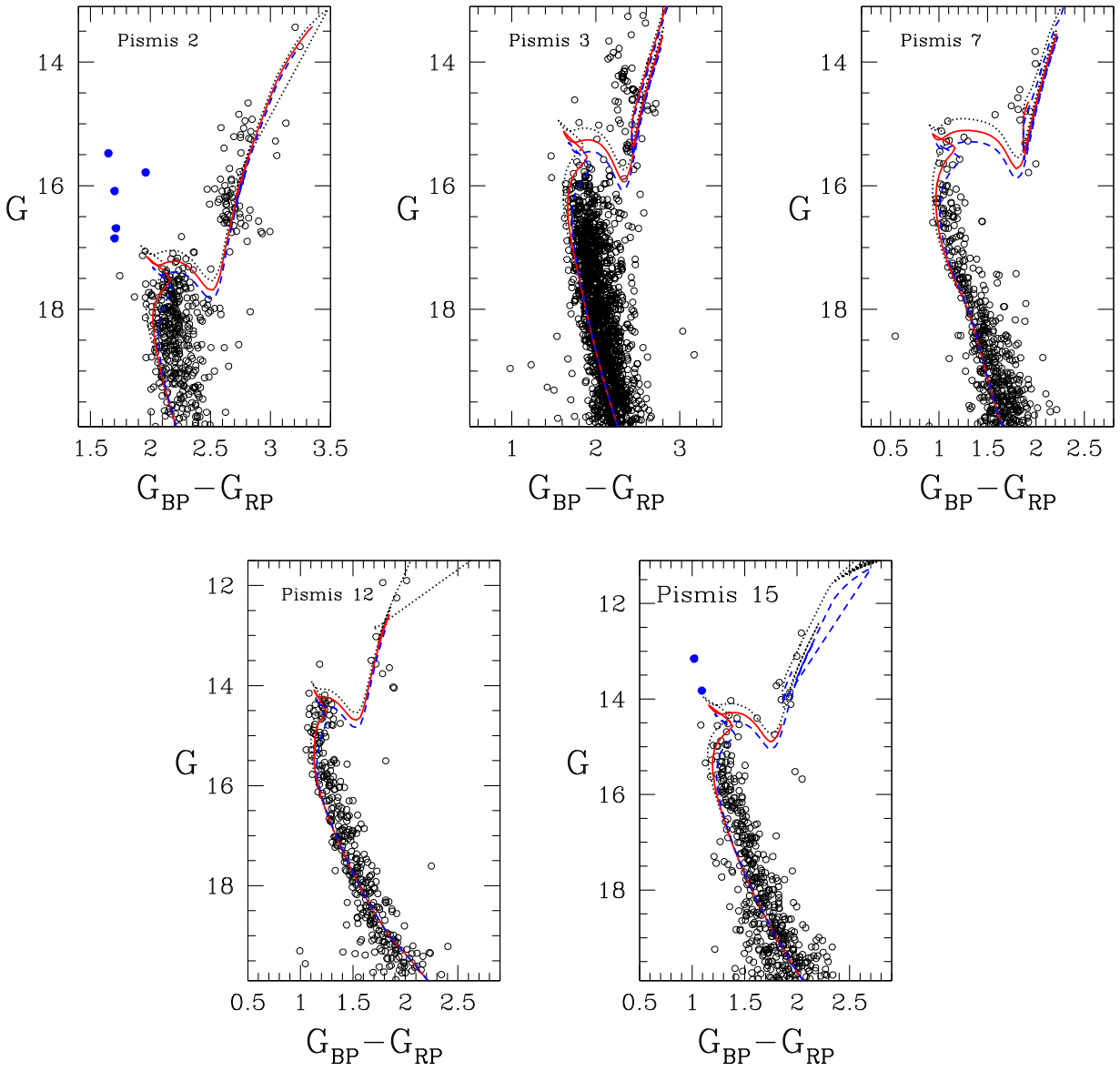

Figure 12. CMD of the clusters under study. All stars are probable members with a membership probability higher than 90%. The curves are the isochrones of (log (age) = 9.25, 9.30, and 9.35) for Pi 2, (log(age) = 9.00, 9.05, and 9.10) for Pi 3, (log(age) = 8.90, 8.95, and 9.00) for Pi 7, (log(age) = 9.35, 9.40, and 9.45) for Pi 12, and (log(age) = 9.10, 9.15, and 9.20) for Pi 15. These ishochrones of metallicity $Z = 0.008$, 0.019, 0.008, 0.019, and 0.008 for clusters Pi 2, Pi 3, Pi 7, Pi 12, and Pi 15, respectively, are taken from Marigo et al. (2017). Blue filled circles are the confirmed member BSSs in Pi 2 and Pi 15.

Table 3
Structural Parameters of the Pismis Clusters under Study

Cluster	R.A. (J2000) (h:m:s)	Central Coordinates decl. (J2000)(d:m:s)	f_0 (stars arcmin^{-2})	f_b (stars arcmin^{-2})	r_c (arcmin)	R_t (pc)
Pismis 2	8:17:55.2	−41:40:12	14.20	0.40	1.92	14.34 ± 0.8
Pismis 3	8:31:19.1	−38:39:00	12.76	3.10	2.07	17.57 ± 1.4
Pismis 7	8:41:10.3	−38:42:3.6	15.58	0.80	1.79	14.96 ± 0.9
Pismis 12	9:20:1.9	−45:7:40.8	10.15	0.52	1.22	11.35 ± 0.8
Pismis 15	9:34:45.1	−48:2:34.8	11.05	0.54	1.38	12.68 ± 0.6

Note. Here the central density, background density, core radius, and tidal radius are represented by f_0, f_b, r_c, and R_t, respectively.

The value of R_h can be estimated based on the transformation equation given in Larsen (2006),

$$R_h = 0.547 \times R_c \times \left(\frac{R_t}{R_c}\right)^{0.486}, \quad (11)$$

where R_c is the core radius and R_t is the tidal radius. We obtained values of half-light radius of 3.14, 2.78, 3.56, 1.58, and 1.95 pc for clusters Pi 2, Pi 3, Pi 7, Pi 12, and Pi 15, respectively.

We estimated the value of T_R as 47, 50, 50, 13, and 20 Myr for Pi 2, Pi 3, Pi 7, Pi 12, and Pi 15, respectively. The

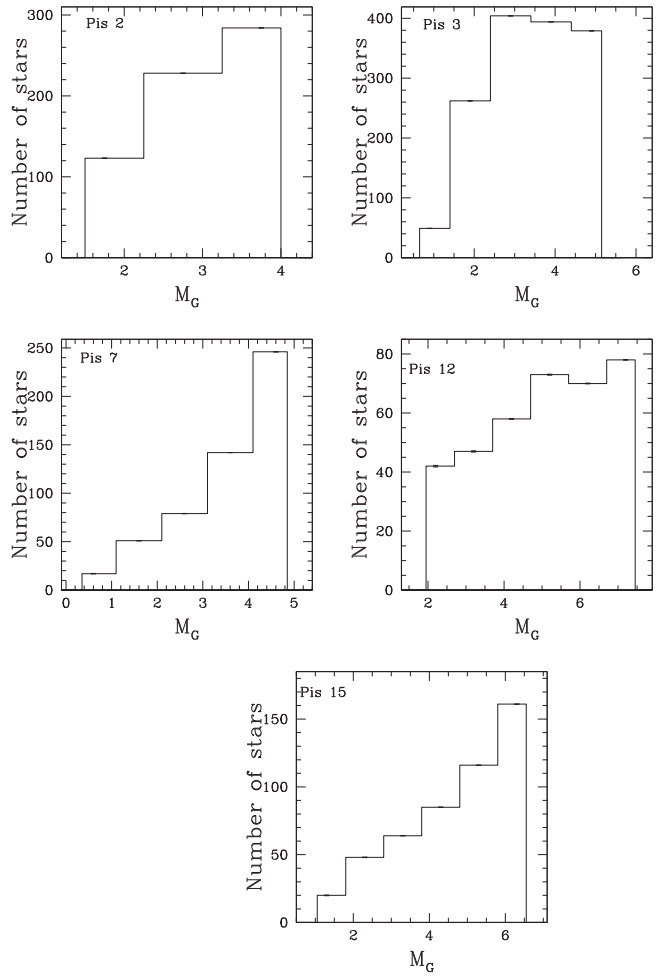

Figure 13. LF of stars in the region of Pismis clusters.

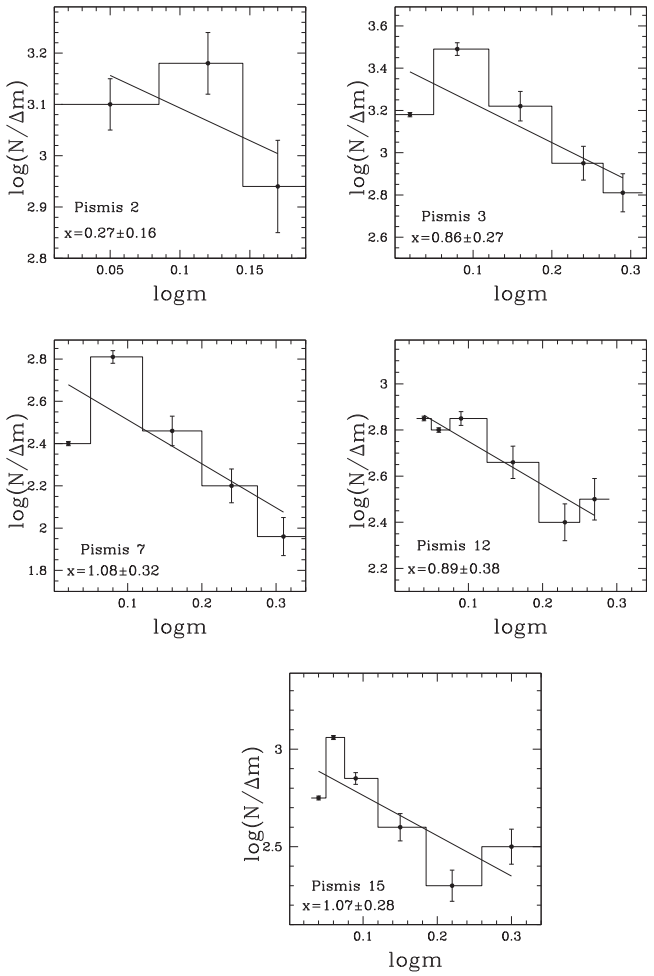

Figure 14. MF histogram derived using the most probable members, where the solid line indicates the power law given by Salpeter (1955).

dynamical evolution parameter ($\tau = \frac{\text{age}}{T_E}$) is found to be much greater than 1 for all clusters, which concludes that these objects are dynamically relaxed.

6.2. Apex of the Pismis Clusters

The apex position represents the motion of the clusters on the celestial sphere. An OC is the gravitationally bound system of stars; member stars of a cluster move with a common velocity vector. We have used the AD diagram method to obtain the apex of Pismis clusters. This method uses radial velocity and parallax of the stars. The AD diagram is discussed in detail by Chupina et al. (2001, 2006), Vereshchagin et al. (2014), Elsanhoury et al. (2018), and Postnikova et al. (2020). The (A, D) values of the individual member stars report the positions of these stars via space velocity vectors. In this method, intersection point ($A_\circ$, $D_\circ$), also called the apex in equatorial coordinates, can be given as

$$A_\circ = \tan^{-1}\left[\frac{\overline{V_y}}{\overline{V_x}}\right], D_\circ = \tan^{-1}\left[\frac{\overline{V_z}}{\sqrt{\overline{V_x}^2 + \overline{V_y}^2}}\right]. \quad (12)$$

Coordinates of the apex ($A_\circ$, $D_\circ$) through the AD diagram method were calculated as ($79\overset{\circ}{.}92 \pm 0\overset{\circ}{.}11$, $22\overset{\circ}{.}87 \pm 0\overset{\circ}{.}15$), ($88\overset{\circ}{.}79 \pm 0\overset{\circ}{.}11$, $27\overset{\circ}{.}66 \pm 0\overset{\circ}{.}15$), ($81\overset{\circ}{.}64 \pm 0\overset{\circ}{.}11$, $18\overset{\circ}{.}66 \pm 0\overset{\circ}{.}15$), ($88\overset{\circ}{.}75 \pm 0\overset{\circ}{.}11$, $10\overset{\circ}{.}19 \pm 0\overset{\circ}{.}15$) and ($87\overset{\circ}{.}01 \pm 0\overset{\circ}{.}13$, $12\overset{\circ}{.}24 \pm 0\overset{\circ}{.}13$) for Pi 2, Pi 3, Pi 7, Pi 12, and Pi 15, respectively. We have also

Table 4
The Main Mass Function Parameters in Clusters

Object	Mass Range ($M_\odot$)	MF Slope	Total Mass ($M_\odot$)	Mean Mass ($M_\odot$)
Pismis 2	1.0–1.6	0.27 ± 0.16	795	1.25
Pismis 3	1.0–2.1	0.86 ± 0.27	1945	1.31
Pismis 7	1.0–2.2	1.08 ± 0.32	760	1.42
Pismis 12	1.0–2.2	0.89 ± 0.38	540	1.46
Pismis 15	1.0–2.1	1.07 ± 0.28	700	1.41

derived several kinematical parameters using techniques represented by Bisht et al. (2020). V_x, V_y, and V_z are spatial velocities of stars on the celestial sphere; x_c, y_c, and z_c are the center coordinates of the clusters; l_A and b_A are the Galactic longitude and latitude of the solar apex; $S_\odot$ is the absolute value of the Sun's velocity relative to the stellar groups under investigation; σ is the velocity dispersion of clusters; L_j and B_j are the Galactic longitude and the Galactic latitude of the directions, respectively, which correspond to the extreme values of the dispersion. All these parameters are listed in Tables 7 and 8. Our estimated kinematical parameters can be critical to understanding the whole picture of a star's space motion for all clusters. The AD diagram for all clusters using

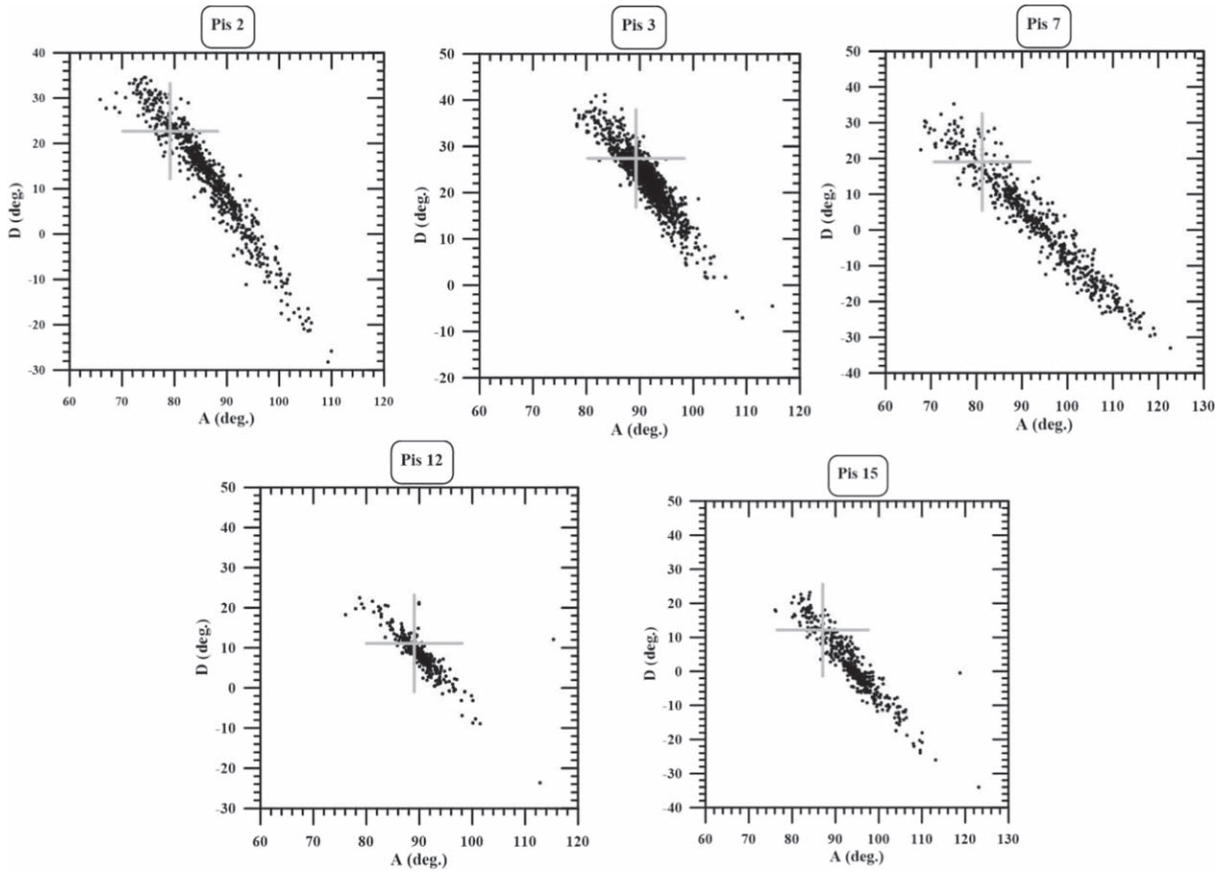

Figure 15. AD diagram for all clusters. All stars are probable members with a membership probability higher than 90%. A plus sign indicates the mean value (Table 7) of apex coordinates.

Table 5
Position and Velocity Components in the Galactocentric Coordinate System

Cluster	R (kpc)	Z (kpc)	U (km s^{-1})	V (km s^{-1})	W (km s^{-1})	ϕ (rad)
Pismis 2	10.078	−0.23	−33.291 ± 0.91	−266.504 ± 2.62	15.273 ± 0.85	0.435
Pismis 3	9.218	0.04	−22.669 ± 0.90	−264.995 ± 1.25	−8.950 ± 0.89	0.283
Pismis 7	10.922	0.22	6.294 ± 3.30	−233.664 ± 2.36	11.940 ± 1.55	0.537
Pismis 12	8.655	0.15	−16.336 ± 2.19	−237.673 ± 0.51	4.968 ± 1.70	0.265
Pismis 15	8.615	0.15	4.404 ± 3.82	−225.856 ± 0.71	3.723 ± 3.57	0.318

Note. Here R is the Galactocentric distance; Z is the vertical distance from the Galactic disk; U, V, W are the radial, tangential, and vertical components of velocity, respectively; and ϕ is the position angle relative to the Sun's direction.

likely members with a membership probability higher than 90% is shown in Figure 15.

7. Orbit Study of the Clusters

7.1. Galactic Potential Model

In this paper, we adopted the approach given by Allen & Santillan (1991) for Galactic potentials in clusters Pi 2, Pi 3, Pi 7, Pi 12, and Pi 15. According to the used model, the Galaxy's mass is expressed by three components: spherical central bulge, massive spherical halo, and disk. Recently, Bajkova & Bobylev (2016) and Bobylev et al. (2017) refined the parameters of potential Galactic models using new observational data for a distance $R \sim 0$–200 kpc. These potentials are given as

$$\Phi_b(r, z) = -\frac{M_b}{\sqrt{r^2 + b_b^2}}$$
$$\Phi_d(r, z) = -\frac{M_d}{\sqrt{r^2 + (a_d + \sqrt{z^2 + b_d^2})^2}}$$
$$\Phi_h(r, z) = -\frac{M_h}{a_h} ln\left(\frac{\sqrt{r^2 + a_h^2} + a_h}{r}\right), \quad (13)$$

where Φ_b, Φ_d, and Φ_h are the potentials of the Galaxy's central bulge, disk, and halo. r and z are the distances of objects from

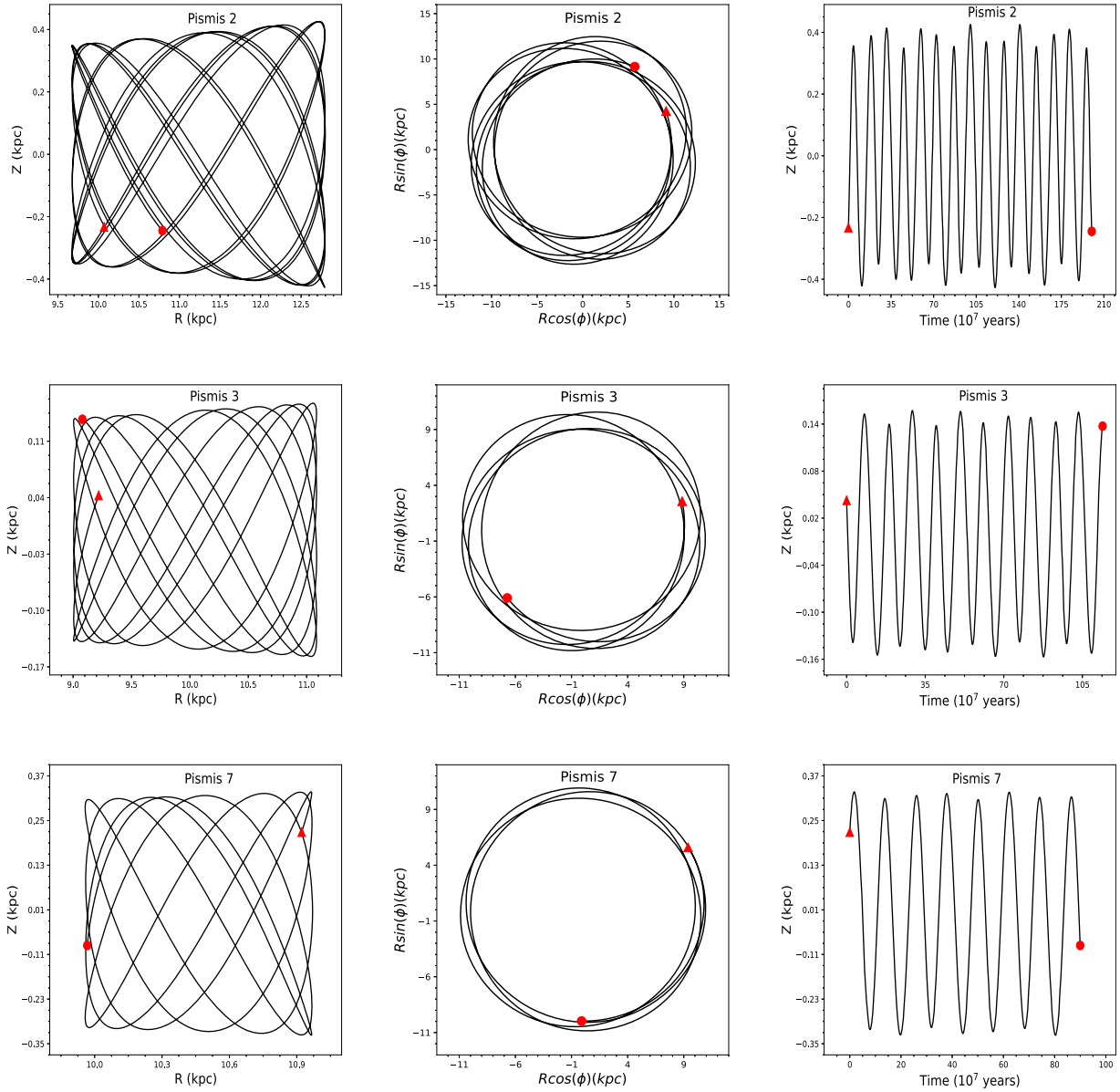

Figure 16. Galactic orbits of the clusters Pi 2, Pi 3, and Pi 7 are estimated with the Galactic potential model described in text in the time interval of the age of the cluster. The left panels show the side view, and the middle panels show the top view of the orbits. The right panels show the motion of clusters in the Galactic disk with time. The filled triangles and circles denote the birth and the present-day positions of the clusters in the Galaxy.

the Galactic center and Galactic disk, respectively. The halo potential is taken from Wilkinson & Evans (1999), and values of the constants are taken from Bajkova & Bobylev (2016).

7.2. Orbit Calculation

The main fundamental parameters (cluster center (α and δ), mean PMs ($\mu_\alpha \cos\delta$, μ_δ), parallax, age, and heliocentric distance ($d_\odot$)) have been used to determine the orbital parameters in the clusters under study. We have used the radial velocity values as 58.99 ± 1.69 km s^{-1}, 30.33 ± 0.25 km s^{-1}, 74.40 ± 1.04 km s^{-1}, 32.445 ± 0.50 km s^{-1}, and 36.28 ± 0.68 km s^{-1} for clusters Pi 2, Pi 3, Pi 7, Pi 12, and Pi 15, respectively, as taken from the catalog given by Soubiran et al. (2018).

We have transformed equatorial space and velocity components into Galactic-space velocity components. The Galactic center is considered at ($17^h45^m32^s.224$, $-28°56'10''$), and the north Galactic pole is considered at ($12^h51^m26^s.282$, $27°7'42''$) (Reid & Brunthaler 2004). To apply a correction for standard solar motion and motion of the local standard of rest (LSR), we used position coordinates of the Sun as (8.3, 0, 0.02) kpc and its velocity components as (11.1, 12.24, 7.25) km s^{-1} (Schönrich et al. 2010). Transformed parameters in the Galactocentric coordinate system are listed in Table 5.

Figures 16 and 17 show the orbits of the clusters Pi 2, Pi 3, Pi 7, Pi 12, and Pi 15. The left panel indicates the motion of the cluster in terms of distance from the Galactic center and Galactic plane, and this shows a 2D side view of the orbits. In the middle panel, the cluster motion is described in terms of x and y components of Galactocentric distance, which shows a top view of orbits. The right panel indicates the motion of clusters under study in the Galactic disk with time. All clusters follow a boxy pattern according to our analysis. Our obtained

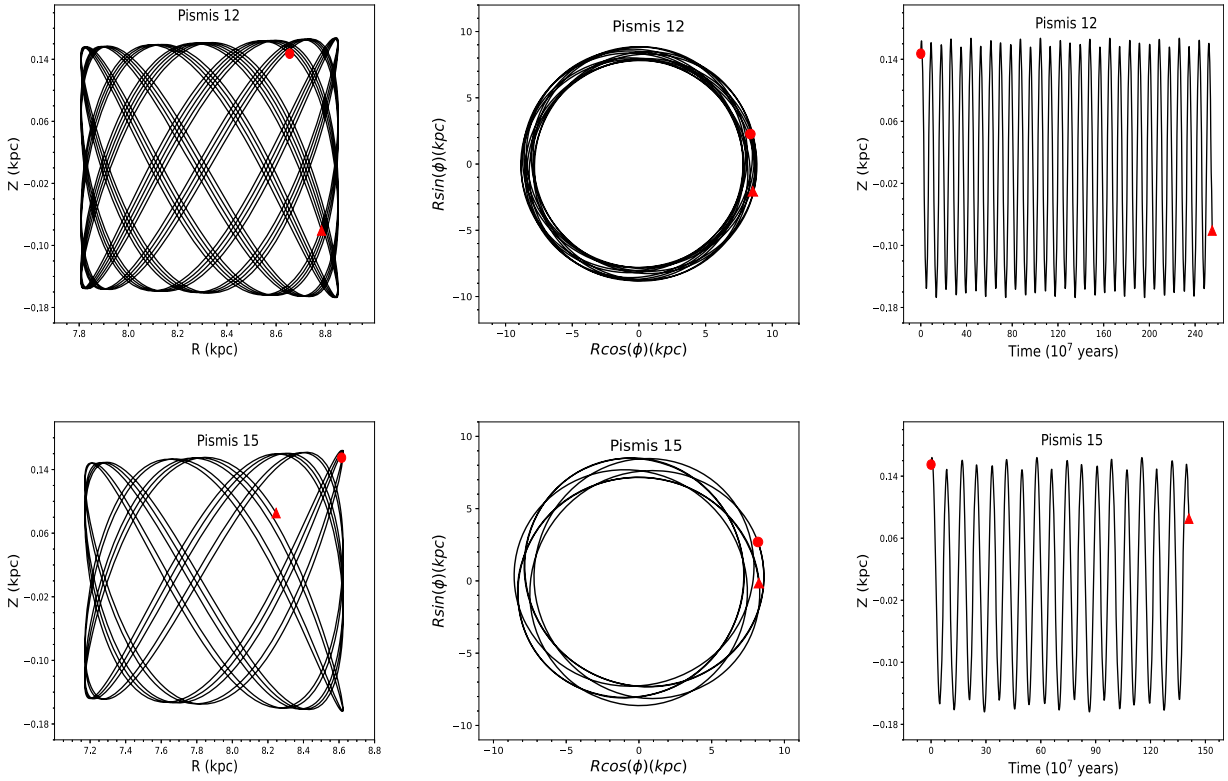

Figure 17. Same as Figure 16, but for clusters Pi 12 and Pi 15.

Table 6
Orbital Parameters Obtained for Pismis Clusters Using the Galactic Potential Model

Cluster	e	R_a (kpc)	R_p (kpc)	$Z_{\max}$ (kpc)	E (100 km s^{-1})^2	J_z (100 kpc km s^{-1})	T_R (Myr)	T_Z (Myr)
Pismis 2	0.004	12.359	12.464	0.425	−9.219	−26.857	236	102
Pismis 3	0.010	10.914	10.566	0.157	−9.844	−24.429	217	92
Pismis 7	0.001	10.940	10.919	0.327	−9.619	−25.520	292	112
Pismis 12	0.000	8.843	08.849	0.167	−10.927	−20.571	227	86
Pismis 15	0.005	8.597	08.503	0.164	−11.241	−19.456	238	86

Note. Here e is eccentricity, R_a is apogalactic distance, R_p is perigalactic distance, $Z_{\max}$ is maximum distance of clusters from the Galactic plane, E is total energy, J_z is angular momemtum, T_R is time period around Galactic center, and T_Z is vertical time period of clusters.

eccentricity values are nearly zero for all studied objects, demonstrating that the target clusters trace a circular path around the Galactic center. The birth and present-day position in the Galaxy are represented by a filled triangle and circle as shown in Figures 16 and 17, respectively. The various orbital parameters have been obtained for these clusters, which are listed in Table 6. Here e is eccentricity, R_a is the apogalactic distance, R_p is perigalactic distance, $Z_{\max}$ is the maximum distance traveled by the cluster from Galactic disk, E is the average energy of orbits, J_z is the z component of angular momentum, T_R is the time period of the revolution around the Galactic center, and T_Z is the time period of vertical motion.

All the clusters are located outside the solar circle (assumed distance of the Sun from the Galactic center is 8.3 kpc) and above 0.15 kpc from the Galactic disk except Pi 3, which is located at 0.04 kpc from the Galactic disk. Among all five clusters, the orbit of Pi 3 is tracing the lowest distance from the Galactic disk. We found that except Pi 3, all the clusters still have most of their fainter stars bound with the clusters as visible in the LFs. But Pi 3 has lost some of its fainter members besides having similar ages to the other clusters. This is because this cluster is close to the Galactic disk and is more affected by the Galactic tidal forces.

8. Conclusions

We delivered a comprehensive photometric and kinematic study of five poorly studied intermediate-age OCs, Pi 2, Pi 3, Pi 7, Pi 12, and Pi 15, using Gaia EDR3 data. We have evaluated the membership probabilities in the region of these clusters and identified the most probable members with membership probabilities higher than 90%. We have utilized these members only to derive the fundamental parameters. In addition, we also shed some light on these clusters' dynamical and kinematical aspects. The main points of the present analysis are as follows:

1. The new obtained central coordinates are foumd as $\alpha = 124.483 \pm 0.06$ deg ($8^{\rm h}17^{\rm m}55\overset{\rm s}{.}9$) and $\delta = -41.674 \pm 0.04$ deg ($-41°40'26\overset{''}{.}4$) for Pi 2, $\alpha = 127.826 \pm 0.09$ deg ($8^{\rm h}31^{\rm m}18\overset{\rm s}{.}2$) and $\delta = -38.650 \pm 0.07$ deg ($-38°39'00''$) for Pi 3, $\alpha = 130.293 \pm 0.08$ deg ($8^{\rm h}41^{\rm m}10\overset{\rm s}{.}3$) and

Table 7
Our Obtained Kinematical Parameters for Pismis Clusters under Study

Parameters	Pismis 2	Pismis 3	Pismis 7
$(A_o, D_o)^o$	79.92 ± 0.11, 22.87 ± 0.15	88.79 ± 0.11, 27.66 ± 0.15	81.64 ± 0.11, 18.66 ± 0.15
$(\overline{V}_x, \overline{V}_y, \overline{V}_z)$ (km s^{-1})	41.02 ± 6.40, 230.75 ± 15.19, 98.87 ± 9.94	2.30 ± 1.51, 108.57 ± 10.42, 56.93 ± 7.55	35.53 ± 5.96, 241.73 ± 15.55, 82.52 ± 9.08
$(\sigma_1, \sigma_2, \sigma_3)$ (km s^{-1})	624.08 ± 24.98, 54.22 ± 7.36, 29.84 ± 5.46	568.66 ± 23.85, 29.98 ± 5.48, 6.38 ± 2.53	1205.90 ± 34.73, 73.61 ± 8.58, 67.68 ± 8.23
$(l_1, m_1, n_1)^o$	0.9758, −0.1600, 0.1495	0.9788, −0.1994, −0.0473	0.9714, −0.1669, 0.1688
$(l_2, m_2, n_2)^o$	−0.1655, −0.9859, 0.0257	−0.2039, −0.9705, −0.1288	−0.1065, 0.9420, 03185
$(l_3, m_3, n_3)^o$	0.1432, −0.0498, −0.9884	0.0200, −0.1356, 0.9906	0.2122, 0.2914, −0.9328
(x_c, y_c, z_c) (kpc)	-3.097 ± 0.06, 4.510 ± 0.07, -4.870 ± 0.07	-1.457 ± 0.04, 1.877 ± 0.04, -1.900 ± 0.04	-6.046 ± 0.08, 7.133 ± 0.08, -7.490 ± 0.09
$(L_j)^o$, $j = 1, 2, 3$	9.307 ± 3.05, 99.530 ± 9.98, -160.826 ± 12.68	11.516 ± 3.39, 101.866 ± 10.09, -98.369 ± 9.92	9.752 ± 3.12, 96.453 ± 9.82, 126.060 ± 11.23
$(B_j)^o$, $j = 1, 2, 3$	8.596 ± 2.93, 1.472 ± 1.21, -81.277 ± 9.02	-2.695 ± 1.64, -7.400 ± 2.72, 82.120 ± 9.06	9.719 ± 3.12, -18.571 ± 4.31, -68.872 ± 8.30
$S_\odot$ (km s^{-1})	254.36 ± 15.95	122.61 ± 11.07	257.89 ± 16.06
$(l_A, b_A)^o$	−2.09, 8.40	−2.21, −0.94	−6.55, 9.32

Note. We have explained the meaning of all parameters in Section 6.2.

Table 8
Same as Table 7, but for Clusters Pi 12 and Pi 15

Parameters	Pismis 12	Pismis 15
$(A_o, D_o)^o$	88.75 ± 0.11, 10.19 ± 0.15	87.01 ± 0.13, 12.24 ± 0.13
$(\overline{V}_x, \overline{V}_y, \overline{V}_z)$ (km s^{-1})	2.26 ± 1.50, 103.26 ± 10.16, 18.56 ± 4.31	9.06 ± 3.01, 175.54 ± 13.25, 38.14 ± 6.18
$(\sigma_1, \sigma_2, \sigma_3)$ (km s^{-1})	121.04 ± 11.00, 16.81 ± 4.10, 3.64 ± 1.91	780.07 ± 27.93, 35.47 ± 5.96, 19.14 ± 4.37
$(l_1, m_1, n_1)^o$	0.9647, 0.2195, 0.1457	0.9870, 0.0626, 0.1478
$(l_2, m_2, n_2)^o$	−0.1987, 0.9693, −0.1448	−0.0627, 0.9980, −0.0041
$(l_3, m_3, n_3)^o$	0.1730, −0.1108, −0.9787	0.1478, 0.0053, −0.9890
(x_c, y_c, z_c) (kpc)	-1.368 ± 0.04, 1.148 ± 0.03, -1.794 ± 0.04	-3.168 ± 0.06, 2.330 ± 0.05, -4.376 ± 0.07
$(L_j)^o$, $j = 1, 2, 3$	-12.817 ± 3.58, -101.582 ± 10.08, -147.364 ± 12.14	-3.630 ± 1.91, -93.595 ± 9.67, 177.967 ± 13.34
$(B_j)^o$, $j = 1, 2, 3$	8.375 ± 2.89, -8.3268 ± 2.89, -78.147 ± 8.84	8.500 ± 2.92, -0.2335 ± 0.48, -81.497 ± 9.03
$S_\odot$ (km s^{-1})	104.94 ± 10.24	179.86 ± 13.41
$(l_A, b_A)^o$	−17.46, 7.68	−14.83, 8.13

$\delta = -38.701 \pm 0.06$ deg ($-38°42'3\farcs6$) for Pi 7, $\alpha = 140.008 \pm 0.08$ deg ($9^h20^m1\fs9$) and $\delta = -45.128 \pm 0.05$ deg ($-45°7'40\farcs8$) for Pi 12, and $\alpha = 143.688 \pm 0.10$ deg ($9^h34^m45\fs1$) and $\delta = -48.043 \pm 0.06$ deg ($-48°2'34\farcs8$) for Pi 15.

2. Cluster radius is estimated as $5\farcm5$, $6\farcm5$, $4\farcm5$, $5\farcm5$, and $6\farcm5$ for clusters Pi 2, Pi 3, Pi 7, Pi 12, and Pi 15, respectively, using RDPs.
3. On the basis of VPD and membership probability estimation of stars, we identified 635, 1488, 535, 368, and 494 most probable cluster members for Pismis clusters. We obtained PM values of (-4.723 ± 0.23 and 5.334 ± 0.24) mas yr^{-1}, (-4.776 ± 0.17 and 6.710 ± 0.19) mas yr^{-1}, (-3.204 ± 0.21 and 2.814 ± 0.24) mas yr^{-1}, (-6.707 ± 0.21 and 4.909 ± 0.20) mas yr^{-1}, and (-5.248 ± 0.25 and 3.432 ± 0.33) mas yr^{-1} for clusters Pi 2, Pi 3, Pi 7, Pi 12, and Pi 15, respectively.
4. A theoretical isochrone given by Marigo et al. (2017) provides an age of 2.0 ± 0.22 Gyr, 1.1 ± 0.12 Gyr, 0.9 ± 0.10 Gyr, 2.5 ± 0.30 Gyr, and 1.4 ± 0.19 Gyr for clusters Pi 2, Pi 3, Pi 7, Pi 12, and Pi 15, respectively. Our obtained distance values are 4.50 ± 0.4 kpc, 2.67 ± 0.3 kpc, 5.10 ± 0.4 kpc, 2.15 ± 0.4 kpc, and 2.50 ± 0.3 kpc for respective clusters using parallax of stars.
5. We have detected five- and two-member BSSs in Pi 2 and Pi 15, respectively, and we found that the identified BSSs are centrally concentrated.
6. The LFs and MFs are determined by considering the most probable cluster members for all clusters under study. The MF slopes are found to be 0.27 ± 0.16, 0.86 ± 0.27, 1.08 ± 0.32, 0.89 ± 0.38, and 1.07 ± 0.28 for clusters Pi 2, Pi 3, Pi 7, Pi 12, and Pi 15, respectively. All the clusters have a flatter MF slope than the Salpeter value. The acquired values of slopes suggest a possibility of dynamical evolution in the studied clusters.
7. The apex coordinates (A_o, D_o) through the AD diagram method were calculated as ($79\fdg92 \pm 0\fdg11$, $22\fdg87 \pm 0\fdg15$), ($88\fdg79 \pm 0\fdg11$, $27\fdg66 \pm 0\fdg15$), ($81\fdg64 \pm 0\fdg11$, $18\fdg66 \pm 0\fdg15$), ($88\fdg75 \pm 0\fdg11$, $10\fdg19 \pm 0\fdg15$), and ($87\fdg01 \pm 0\fdg13$, $12\fdg24 \pm 0\fdg13$) for Pi 2, Pi 3, Pi 7, Pi 12, and Pi 15, respectively.
8. We have derived the velocity ellipsoid parameters, direction cosines (l_j, m_j, n_j), Galactic longitude of the vertex (l_2), and solar elements for all clusters, which are listed in Tables 7 and 8.
9. Galactic orbits and orbital parameters are estimated using Galactic potential models for Pismis clusters. We found that all objects orbit in a boxy pattern in a circular orbit.

The different orbital parameters are listed in Tables 5 and 6 for the clusters under study.

The authors thank the anonymous referee for the useful comments that significantly improved the article's scientific content. This work has been supported by the Natural Science Foundation of China (NSFC-11590782, NSFC-11421303). D. P.S. and I.-G.J. are supported by the grant from the Ministry of Science and Technology (MOST), Taiwan. The grant numbers are MOST 105-2119-M-007-029 -MY3, and MOST 106-2112-M-007-006 -MY3. W.H.E. extends their appreciation to the Deputyship for Research & Innovation, Ministry of Education in Saudi Arabia, for funding this research work through project No. IF-2020-NBU-104. This work has made use of data from the European Space Agency (ESA) mission Gaia (https://www.cosmos.esa.int/gaia), processed by the Gaia Data Processing and Analysis Consortium (DPAC, https://www.cosmos.esa.int/web/gaia/dpac/consortium). Funding for the DPAC has been provided by national institutions, particularly the institutions participating in the Gaia Multilateral Agreement. In addition, it is worth mentioning that this work has been done using WEBDA.

ORCID iDs

D. Bisht https://orcid.org/0000-0002-8988-8434
Qingfeng Zhu https://orcid.org/0000-0003-0694-8946
W. H. Elsanhoury https://orcid.org/0000-0002-2298-4026
Geeta Rangwal https://orcid.org/0000-0002-6373-770X
Devesh P. Sariya https://orcid.org/0000-0001-8452-7667
Ing-Guey Jiang https://orcid.org/0000-0001-7359-3300

References

Ahumada, J., & Lapasset, E. 1995, A&AS, 109, 375
Ahumada, J. A. 2005, AN, 326, 3A
Allen, C., & Santillan, A. 1991, RMxAA, 22, 255
Angelo, M. S., Santos, J. F. C., & Corradi, W. J. B. 2020, MNRAS, 493, 3473
Balaguer-Núñez, L., Tian, K. P., & Zhao, J. L. 1998, A&AS, 133, 387
Bastian, N., Covey, K. R., & Meyer, M. R. 2010, ARA&A, 48, 339
Bailer-Jones, C. A. L. 2015, PASP, 127, 994
Bailer-Jones, C. A. L., Rybizki, J., Fouesneau, M., Mantelet, G., & Andrae, R. 2018, AJ, 156, 58
Bisht, D., Elsanhoury, W. H., Zhu, Q., et al. 2020, AJ, 160, 119B
Bisht, D., Yadav, R. K. S., Ganesh, S., et al. 2019, MNRAS, 482, 1471B
Bisht, D., Zhu, Q., Yadav, R. K. S., et al. 2021a, AJ, 161, 182
Bisht, D., Zhu, Q., Yadav, R. K. S., et al. 2021b, MNRAS, 503, 5929
Bisht, D., Zhu, Q., Yadav, R. K. S., et al. 2022, PASP, 134d, 4201B
Bajkova, A. T., & Bobylev, V. V. 2016, AstL, 42, 9
Bobylev, V. V., Bajkova, A. T., & Gromov, A. O. 2017, AstL, 43, 4
Bica, E., & Bonatto, C. 2011, A&A, 530A, 32B
Cakmak, H., Gunes, O., Karatas, Y., & Bonatto, C. 2021, AN, 342, 975C
Cantat-Gaudin, T., Anders, F., Castro-Ginard, A., et al. 2020, A&A, 640, A1
Cantat-Gaudin, T., Jordi, C., Vallenari, A., et al. 2018, A&A, 618, A93
Carraro, G., Geister, D., Baume, G., Vázquez, R., & Moitinho, A. 2005, MNRAS, 360, 655
Carraro, G., & Ortolani, S. 1994, A&A, 291, 106
Chumak, Y. O., Platais, I., McLaughlin, D. E., Rastorguev, A. S., & Chumak, O. V. E. 2010, MNRAS, 402, 1841
Chupina, N. V., Reva, V. G., & Vereshchagin, S. V. 2001, A&A, 371, 115
Chupina, N. V., Reva, V. G., & Vereshchagin, S. V. 2006, A&A, 451, 909
Di Fabrizio, L., Bragaglia, A., Tosi, M., & Marconi, G. 2001, MNRAS, 328, 795
Dias, W. S., Alessi, B. S., Moitinho, A., & Lepine, J. R. D. 2002, A&A, 389, 871
Dias, W. S., Monteiro, H., & Assafin, M. 2018a, MNRAS, 478, 5184
Dias, W. S., Monteiro, H., Caetano, T. C., et al. 2014, A&A, 564, A79
Dias, W. S., Monteiro, H., Lépine, J. R. D., et al. 2018b, MNRAS, 481, 3887
Dib, S., & Basu, S. 2018, A&A, 614, A43
Durgapal, A. K., & Pandey, A. K. 2001, A&A, 375, 840
Dutra, C. M., & Bica, E. 2000, A&A, 359, 347D
Eggen, O. J. 1984, AJ, 89, 1350
Elsanhoury, W. H., et al. 2018, Ap&SS, 363, 58
Friel, E. D., & Janes, K. A. 1993, A&A, 267, 75
Friel, E. D. 1995, ARA&A, 33, 381
Friel, E. D., Janes, K. A., Tavarez, M., et al. 2002, AJ, 124, 2693F
Gaia Collaboration, Brown, A. G. A., Vallenari, A., et al. 2021, A&A, 649, A1
Galli, P. A. B., Teixeira, R., Ducourant, C., Bertout, C., & Benevides-Soares, P. 2012, A&A, 538, 23
Genzel, R., & Townes, C. H. 1987, ARA&A, 25, 377
Girard, T. M., Grundy, W. M., Lopez, C. E., & van Altena, W. F. 1989, AJ, 98, 227
Gunn, J. E., Griffin, R. F., Griffin, R. F. M., & Zimmerman, B. A. 1988, AJ, 97, 198
Hanson, R. B. 1975, AJ, 80, 379
He, Z.-H., Xu, Y., & Hou, L.-G. 2021, RAA, 21, 009
Hou, L. G. 2021, FrASS, 8, 103
Janes, K. A. 1988, In Calibration of Stellar Ages (Schenectady, NY: L. Davis Press), 59
Janes, K. A., & Phelps, R. L. 1994, AJ, 108, 1773J
Jeřábková, T., Hasani Zonoozi, A., Kroupa, P., et al. 2018, A&A, 620, A39
Johnson, H. L., & Sandage, A. R. 1955, ApJ, 121, 616
Kharchenko, N. V., Piskunov, A. E., Schilbach, S., Roeser, S., & Scholz, R. D. 2013, A&A, 558A, 53K
Kharchenko, N. V., Piskunov, A. E., Schilbach, S., Roeser, S., & Scholz, R. D. 2016, A&A, 585A, 101K
Kim, S. C., Kyeong, J., Park, H. S., et al. 2017, JKAS, 50, 79K
Kim, S. S., Figer, D. F., Lee, H. M., & Morris, M. 2000, ApJ, 545, 301
King, I. 1962, AJ, 67, 471
Kjeldsen, H., & Frandsen, S. 1991, A&AS, 87, 119
Lada, C. J., & Lada, E. A. 2003, ARAA, 41, 57
Larsen, S. S. 2006, arXiv:astro-ph/0701774
Larson, R. B. 1998, MNRAS, 301, 569L
Lindegren, L., Bastian, U., Biermann, M., et al. 2020, A&A, 640, A1
Liu, L., & Pang, X. 2019, ApJS, 245, 32
Massey, P., Johnson, K. E., & DeGioia-Eastwood, K. 1995, ApJ, 454, 151
Marigo, P., Girardi, L., Bressan, A., et al. 2017, ApJ, 835, 77
Miller, N. A., Hong, L. N., Friel, E. D., & Janes, K. A. 1995, BAAS, 27, 1438M
Pandey, A. K., Sharma, S., Upadhyay, K., et al. 2007, PASJ, 59, 547
Portegies Zwart, S. F., McMillan, S. L. W., & Gieles, M. 2010, ARA&A, 48, 431
Phelps, R. L., & Janes, K. A. 1993, AJ, 106, 1870
Phelps, R. L., Janes, K. A., & Montgomery, K. A. 1994, AJ, 107, 1079P
Postnikova, E. S., Elsanhoury, W. H., Devesh, P., et al. 2020, RAA, 20, 16
Reid, M. J., & Brunthaler, A. 2004, ApJ, 616, 872
Röser, S., Demleitner, M., & Schilbach, E. 2010, AJ, 139, 2440
Sagar, R., Myakutin, V. I., Piskunov, A. E., & Dluzhnevskaya, O. B. 1988, MNRAS, 234, 831
Salpeter, E. E. 1955, ApJ, 121, 161
Sampedro, L., Dias, W. S., Alfaro, E. J., Monteiro, H., & Molino, A. 2017, MNRAS, 470, 3937S
Sandage, A. R. 1962, ApJ, 135, 333
Sariya, D. P., Jiang, I.-G., Bisht, D., Yadav, R. K. S., & Rangwal, G. 2021, AJ, 161, 102
Sariya, D. P., Jiang, I.-G., & Yadav, R. K. S. 2018, RAA, 18, 126
Soubiran, C., Cantat-Gaudin, T., Romero-Gómez, M., et al. 2018, A&A, 619, A155
Spitzer, L., & Hart, M. 1971, ApJ, 164, 399
Schönrich, R., Binney, J., & Dehnen, W. 2010, MNRAS, 403, 1829
Vereshchagin, S. V., Chupina, N. V., Sariya, D. P., Yadav, R. K. S., & Kumar, B. 2014, NewA, 31, 43
von Hoerner, S. 1957, ApJ, 125, 451
Wayman, P. A., Symms, L. S., & Blackwell, K. C. 1965, R. Obs. Bull, 1965, 98
Wilkinson, M. I., & Evans, N. W. 1999, MNRAS, 310, 645
Xu, Y., Hou, L.-G., & Wu, Y.-W. 2018, RAA, 18, 146
Yadav, R. K. S., Sariya, D. P., & Sagar, R. 2013, MNRAS, 430, 3350